

JGR Atmospheres

RESEARCH ARTICLE

10.1029/2022JD038119

Key Points:

- The optimized model with ozone-vegetation coupling improves the simulations of vegetation physiology and dry deposition velocity in China
- The O₃-damaged photosynthesis and stomatal conductance could affect regional meteorology, finally contributing to surface ozone increase
- The ozone-vegetation coupling constitutes complex feedbacks on ozone itself by altered meteorology, biogenic emissions and dry deposition

Supporting Information:

Supporting Information may be found in the online version of this article.

Correspondence to:

M. Li,
mengmengli2015@nju.edu.cn

Citation:

Jin, Z., Yan, D., Zhang, Z., Li, M., Wang, T., Huang, X., et al. (2023). Effects of elevated ozone exposure on regional meteorology and air quality in China through ozone-vegetation coupling. *Journal of Geophysical Research: Atmospheres*, 128, e2022JD038119. <https://doi.org/10.1029/2022JD038119>

Received 3 NOV 2022

Accepted 16 MAR 2023

Effects of Elevated Ozone Exposure on Regional Meteorology and Air Quality in China Through Ozone-Vegetation Coupling

Zhipeng Jin¹, Dan Yan¹, Zihan Zhang¹, Mengmeng Li^{1,2} , Tijian Wang¹ , Xin Huang¹, Min Xie¹ , Shu Li¹ , and Bingliang Zhuang¹ 

¹School of Atmospheric Sciences, Nanjing University, Nanjing, China, ²Frontiers Science Center for Critical Earth Material Cycling, Nanjing, China

Abstract Ozone is a phytotoxic pollutant that could damage the vegetation growth and lead to complicated impacts on air quality through meteorological and biogeochemical feedbacks. This study implements a semi-empirical parameterization regarding the impacts of ozone exposure on photosynthesis rate and stomatal resistance into the Noah-Multi-parameterization (Noah-MP) dynamic vegetation module of Weather Research and Forecasting with Chemistry (WRF/Chem) model. The gaseous dry deposition and biogenic emission algorithms are also coupled with Noah-MP to enable the ozone-vegetation coupling. This model reproduces the near-surface meteorology, air pollutants and vegetation physiology in China, with a spatial correlation coefficient more than 0.9 and normalized mean bias from -0.19 to 0.42. The optimized model also improves the simulations of vegetation physiology (e.g., a reduction of model error by 18%–32%) and ozone dry deposition velocity. The elevated ozone damages plant photosynthesis, and decreases the national gross primary productivity (-28.85%) and leaf area index (-17.41%). The plant transpiration and surface heat flux, as well as air temperature (e.g., up to +0.16°C in summer) and other associated meteorological variables are also altered, finally contributing to 0.49 µg m⁻³ increase of surface ozone. Otherwise, the suppressed vegetation LAI and biogenic emissions, as well as the lower dry deposition velocity in response to the ozone-vegetation coupling contribute to the remaining ozone changes by -1.07 µg m⁻³ and 1.18 µg m⁻³, jointly constituting the complicated ozone-vegetation feedbacks on air quality. Our results highlight the necessity of including the ozone-vegetation coupling in models for reliable prediction of regional climate and air quality.

Plain Language Summary Vegetation controls the land-atmosphere carbon/water cycle and material exchange, and is thus important in global/regional climate and atmospheric environment. Chronic exposure to ozone could damage the vegetation growth and lead to complicated impacts on regional climate and air quality. This study considers the impacts of ozone exposure on plant photosynthesis and stomata using a semi-empirical parameterization into the WRF/Chem-Noah-MP regional meteorology-chemistry-vegetation coupled model. The model well reproduces the near-surface meteorology, air pollutants and vegetation characteristics in China, with moderate model improvements due to the optimized dynamic vegetation and dry deposition modules. The elevated ozone damages plant photosynthesis and decreases the national gross primary productivity (-28.85%) and leaf area index (-17.41%). Otherwise, the plant transpiration and surface heat flux, as well as air temperature (e.g., up to +0.16°C in summer) and other associated meteorological variables are also altered. The meteorological changes, along with the suppressed biogenic emissions from vegetation and lower dry deposition velocity due to the ozone-vegetation damage jointly constitute the complicated ozone-vegetation feedbacks on air quality and contribute to an average of -1.1~1.2 µg m⁻³ surface ozone change. Our results highlight the necessity of including the ozone-vegetation coupling for reliable model predictions.

1. Introduction

Terrestrial vegetation directly controls the carbon and water cycle between the biosphere and atmosphere (Avise et al., 2009; Sanderson et al., 2003), and also constraints the material exchange and stomatal deposition of atmospheric composition (Papanatsiou et al., 2017; Yang et al., 2021), making terrestrial vegetation play an essential role in global climate and atmospheric chemistry. Ozone (O₃) is an important phytotoxic pollutant in the atmosphere (Calatayud et al., 2007; Fiscus et al., 2005; Herbinger et al., 2007). The ambient ozone could enter the leaf through stomata and generate reactive oxygen species in the apoplast (Iriti & Faoro, 2008; Kangasjärvi et al., 2005). Once the uncontrolled oxidative burst from the breakdown of ozone exceeds the apoplastic

antioxidative capacity, it may cause injury to biomacromolecules and cell death, and induce stomatal closure of plant as a protective mechanism (Hoshika et al., 2015). Chronic exposure to elevated ozone could damage the plant transpiration, and modulate the water/heat fluxes and climate (J Li et al., 2016; Mills et al., 2009) or suppress the plant photosynthesis and carbon sequestration (Ainsworth et al., 2012; Sitch et al., 2007), further exerting profound impacts on global/regional climate and atmospheric environment.

Past studies have widely discussed the impacts of ozone on plant productivity (Ren et al., 2011; Van Dingenen et al., 2009; Yue et al., 2017) and carbon cycle (Ainsworth et al., 2012; Lombardozzi et al., 2015; Sitch et al., 2007). For example, decades of observational records demonstrated the effects of surface ozone on vegetation and crop productivity (Ainsworth et al., 2012). Using the Community Land Model (CLM), Lombardozzi et al. (2015) estimated that the present-day O₃ exposure could reduce global gross primary productivity (GPP) by 8%–12%. It was predicted that by 2100 the ozone-induced reduction in global terrestrial carbon sink (143–263 Pg C) through suppressing plant photosynthesis could have an indirect radiative forcing of 0.62–1.09 W m⁻², which is comparable to the greenhouse effect of ozone (0.89 W m⁻²) (Sitch et al., 2007). Ren et al. (2011) analyzed the impacts of tropospheric ozone on the carbon exchange in China's forest ecosystem, and found that the elevated ozone could lead to a reduction of total forest carbon reserve by 7.7% and carbon exchange by 0.4%–43.1%. On the other hand, ozone exposure could also reduce the vegetation-atmosphere water exchange through affecting the leaf stomatal closure, which may have widespread implications for regional climate (Sitch et al., 2007) and hydrology (B S Felzer et al., 2009; Lombardozzi et al., 2015; McLaughlin et al., 2007). The simulations in summer of 2007–2012 found that the surface ozone pollution decreased latent heat flux (LH), precipitation and runoff by 10–27 W m⁻², 0.9–1.4 mm d⁻¹ and 0.1–0.17 mm d⁻¹, and increased surface air temperature by 0.6–2.0°C in Texas and surrounding areas (Cuntz et al., 2016). Lombardozzi et al. (2015) used the CLM model to estimate the impacts of ozone exposure on plant transpiration and runoff. They found that the present-day ozone pollution resulted in a reduction of plant transpiration rate (TR) by 2%–2.4% and an increase of surface runoff by 15% in eastern US, exerting profound impacts on global climate. B S Felzer et al. (2009) found that the ozone-induced stomatal closure could increase the runoff by 6%–11% in the temperate forest of the US, highlighting the important role of ozone in water cycle. Zhu et al. (2022) applied a two-way coupled atmosphere model to simulate the ozone-induced damage in China during summers of 2014–2017, and revealed that the inclusion of ozone-vegetation coupling caused a 5–30 W m⁻² decrease in latent heat flux, 3% reduction in surface humidity and 0.2–0.8°C increase in air temperature.

Despite that, the vegetation-ozone interactions are neglected in most of the current meteorology-chemistry models due to the lack of plant-specific response parameters for the ozone damages on photosynthesis and stomatal conductance. Thus, few studies have explicitly determined the effects of ozone on plant transpiration as well as regional weather/climate in Asia. Additionally, many land surface models assume a tight linear correlation between stomatal conductance and photosynthetic rate, and they calculate the ozone-induced changes in stomatal conductance only dependent on the suppression of photosynthesis rate, thus ignoring the independent damage of ozone on plant stomata (B Felzer et al., 2005; B. S Felzer et al., 2009; Ren et al., 2011; Sitch et al., 2007; Super et al., 2015). But actually the atmospheric oxidative stress caused by ozone would lead to a decouple between the plant photosynthesis and stomatal conductance (Calatayud et al., 2007; Francini et al., 2007; Lombardozzi et al., 2012). Several meta-analyses and reviews pointed out that the ozone-induced decrease in photosynthetic rate is usually larger than stomatal conductance, and even increase stomatal conductance under extreme conditions (Feng et al., 2011; Lombardozzi et al., 2013; Morgan et al., 2003; Wittig et al., 2007). The linear assumption likely overpredicted the decreases in stomatal conductance and thus fail to accurately predict the responses of climatic variables to ozone. Lombardozzi et al. (2012) proposed a parameterized method to describe the ozone damage to plant stomatal conductance and photosynthetic rate independently and improved the climate predictions.

The ozone-vegetation coupling could not only impact the carbon/water cycle and climate, but also shows complex implications for regional air quality. The ozone-vegetation coupling could constitute important feedbacks that ultimately affect ozone air quality itself through disturbing the local weather situations for ozone chemical production and accumulation (i.e., “meteorological feedback”), or through modifying the vegetation phenology and consequently biogenic emissions and deposition of pollutants (i.e., “biogeochemical feedback”) (Gong et al., 2020; Sadiq et al., 2017). For example, ozone exposure can suppress the plant transpiration and modify the surface heat partition, leading to a cascade of meteorological and chemical changes: for example, lower humidity reduces the chemical loss of ozone; higher temperature enhances ozone through increased photochemical reaction rate and

biogenic emission. On the other hand, the reduced deposition caused by lower stomatal conductance and a possible decline in leaf area index (LAI) following ozone exposure can also potentially affect ozone levels. In recent years, some researchers have paid attention to the impacts of ozone-vegetation coupling on atmospheric chemistry. Sadiq et al. (2017) introduced an empirical parameterization of ozone impacts on plant photosynthesis and stomatal conductance in the CESM earth system model; they found that the ozone-vegetation coupling produced $8.6\text{--}12.8 \mu\text{g m}^{-3}$ increase of surface ozone concentration in Europe, North America and China, and 40%–100% of the ozone increase could be attributed to the ozone damage to dry deposition and TR while the enhanced biogenic emission contributes to the remaining ozone increase. Using a global climate-chemistry-carbon coupled model, Gong et al. (2020) also found that the changes in plant stomatal conductance and dry deposition due to ozone exposure resulted in an increase of surface ozone in East China, eastern USA and western Europe by 4.5, 3.9 and $2.8 \mu\text{g m}^{-3}$ and the suppressed biogenic emission alone weakens the positive ozone feedback in western Europe by $2.1\text{--}4.3 \mu\text{g m}^{-3}$. Zhu et al. (2022) found that the meteorological changes induced $4.3\text{--}12.8 \mu\text{g m}^{-3}$ increase in surface O_3 of northern and south-central China in response to the ozone-vegetation coupling, but they ignored the biogeochemical feedback between ozone-vegetation coupling and regional air quality that has been proven to be a major pathway (Gong et al., 2020; Sadiq et al., 2017).

In the recent decade, surface ozone in China has increased significantly with the expanding economy and appeared to be an universal environmental concern (M Li et al., 2021; Verstraeten et al., 2015). Many regions have experienced persistent high ozone exceeding the ecological threshold that could change the carbon/water exchanges between the terrestrial ecosystem and atmosphere (Bonan, 2008; Wittig et al., 2007). However, the strong feedbacks arising from ozone-induced vegetation damage on regional climate and air quality remain poorly characterized before.

Here, we use an online regional meteorology-chemistry model (WRF/Chem) coupled with the Noah-Multi-parameterization (Noah-MP) land model with a dynamic vegetation module to investigate the non-radiative impacts of ozone exposure on regional meteorology and air quality in China through ozone-vegetation coupling. The model configurations and numerical designs are presented in Section 2. Section 3 discusses the results. Finally, a summary is presented in Section 4.

2. Methods and Materials

2.1. WRF/Chem-Noah-MP Model Configurations

2.1.1. Model Setup

This study uses the WRF/Chem model version 4.1 (G Grell et al., 2002) coupled with Noah-MP land surface scheme (Niu et al., 2011) to simulate the meteorology-chemistry-vegetation interactions. Noah-MP is a new-generation land surface model developed from the Noah model (Ek et al., 2003). It contains a dynamic vegetation module to simulate the plant photosynthesis rate and stomatal conductance, carbon partition and plant growth, a simple groundwater model, and a frozen soil scheme (Niu et al., 2011). The Noah-MP model has been widely used in numerical weather prediction (Yoon et al., 2021), regional climate (Barlage et al., 2015) and hydrologic studies (Cuntz et al., 2016). A semi-empirical parameterization of ozone impacts on photosynthesis rate and stomatal conductance is incorporated into the WRF/Chem-Noah-MP model to enable the ozone-vegetation coupling (see Section 2.1.2).

The modeling domain is configured with 211×182 grid cells at 25 km horizontal resolution, which covers the entire mainland China (Figure 1). Anthropogenic emissions are adopted from the 0.25° Multi-resolution Emission Inventory for China (MEIC) and MIX Asian emission inventory for the other regions (available at <http://meicmodel.org>). The atmospheric chemistry is simulated using the Carbon Bond Mechanism version Z (CBMZ) (Zaveri & Peters, 1999) gas-phase chemistry module coupled with the Model for Simulating Aerosol Interactions and Chemistry (Zaveri et al., 2008). The model physical configurations include the YSU boundary layer scheme (Noh et al., 2003), the RRTMG radiation scheme (Iacono et al., 2008), the Grell cumulus scheme (G. A Grell & Dévényi, 2002) and the Thompson microphysics scheme (Thompson et al., 2016).

2.1.2. Plant Responses to Ozone Damage in the Noah-MP Model

In Noah-MP, the plant photosynthetic rate and stomatal conductance are calculated using the Farquhar/Ball-Berry model (Ball et al., 1987; Bonan et al., 2011; Farquhar et al., 1980). It has been commonly used to simulate the

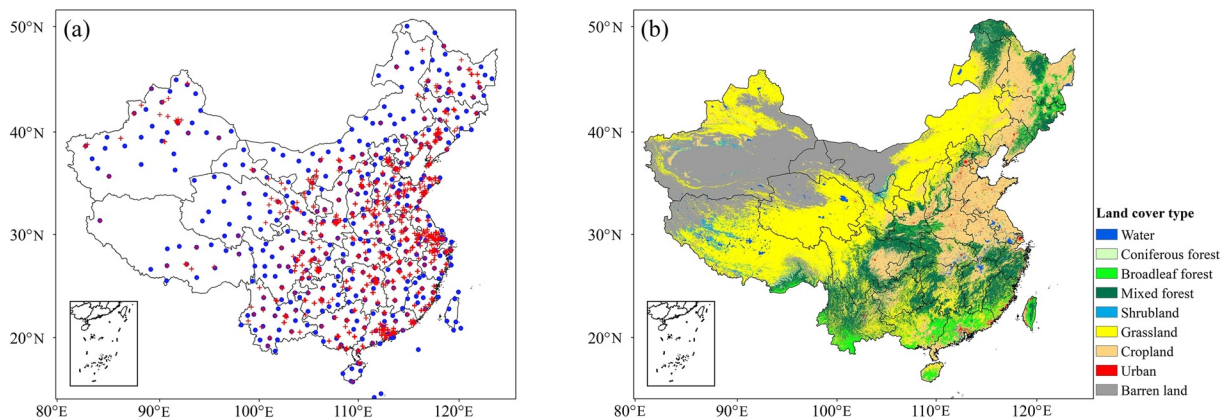


Figure 1. (a) The WRF/Chem-Noah-MP modeling domain and observational stations (red dots: air quality monitoring stations; blue dots: weather stations) across China. (b) Land cover type derived from MODIS satellite data.

plant physiology in regional models and is proven to accurately predict the photosynthesis rate and stomatal conductance over a range of environmental conditions (Collatz et al., 1991; Misson et al., 2004). The Farquhar photosynthesis model expresses the carbon dioxide (CO_2) assimilation rate (A , $\mu\text{g C m}^{-2} \text{s}^{-1}$) as the minimum of three limiting factors (Equation 1).

$$A = \min(A_c, A_j, A_p) \quad (1)$$

where A_c is the Rubisco-limited photosynthesis rate; A_j is the light-limited photosynthesis rate; A_p is that associated with transport of photosynthate.

The carbon assimilation rate through photosynthesis, together with the carbon allocation to leaf and respiration of leaf are then used to dynamically calculate the leaf carbon mass (C_{leaf} , g m^{-2} ; Equation 2) and LAI.

$$\frac{\partial C_{\text{leaf}}}{\partial t} = F_{\text{leaf}} A - (S_{\text{cd}} + T_{\text{leaf}} + R_{\text{leaf}})C_{\text{leaf}} \quad (2)$$
$$\text{LAI} = C_{\text{leaf}} \times m2lai$$

where A is the total carbon assimilation rate calculated in Equation 1; F_{leaf} is the fraction of assimilation carbon allocated to leaf; S_{cd} is the leaf death rate due to cold and drought stresses; T_{leaf} is the leaf turnover rate due to senescence, herbivory or mechanical loss; R_{leaf} is the leaf respiration rate; $m2lai$ is the vegetation-dependent leaf area parameter (m g^{-1}) used to convert C_{leaf} to LAI.

The leaf-level stomatal conductance (g_s , m s^{-1}) is linearly related to photosynthetic rate and is calculated as Equation 3.

$$g_s = b + mAh_s/c_s \quad (3)$$
$$r_s = 1/g_s$$

where b is the minimum stomatal conductance; m is the Ball-Berry slope of the conductance-photosynthesis relationship; h_s is the fractional humidity at the leaf surface; c_s is the ambient CO_2 concentration at the leaf surface; r_s is the leaf-level stomatal resistance calculated as the inverse of stomatal conductance.

Under the oxidative stress, the ozone-modified photosynthesis rate and stomatal conductance are thought to be related to the cumulative O_3 uptake (CUO, mmol m^{-2}) by leaf stomata. Lombardozzi et al. (2012) developed a method to quantify the unequal effects of cumulative O_3 uptake on photosynthesis rate and stomatal conductance, separately, based on the unifying theory. The O_3 -modified photosynthesis rate (F_{AO_3}) and stomatal conductance (F_{GO_3}) are simulated separately using the O_3 damage functions, as shown in Equation 4.

$$F_{AO_3} = a_p + b_p \times \text{CUO} \quad (4)$$
$$F_{GO_3} = a_g + b_g \times \text{CUO}$$

where a_p , b_p , a_g , and b_g are the plant-specific response parameters presented in Lombardozzi et al. (2013) (namely “*Lom13*”) based on literature review (Table S1 in Supporting Information S1). Leaf photosynthesis rate and stomatal conductance are modified by multiplying the initial values calculated using the Farquhar/Ball-Berry formulas by the F_{AO_3} and F_{GO_3} factors.

The cumulative O₃ uptake by leaf stomata is calculated as Equation 5.

$$\text{CUO} = \sum (k_{o_3}/r_s + 1/r_a) \times [O_3] \quad (5)$$

where $k_{o_3} = 1.67$ is the ratio of leaf stomatal resistance to ozone to leaf stomatal resistance to water; r_s is the leaf stomatal resistance calculated using Equation 3; r_a is the aerodynamic and boundary layer resistance; $[O_3]$ is the near-surface O₃ concentration. An uptake of 0.8 nmol O₃ m⁻² s⁻¹ is used as a flux threshold. CUO only accumulates during the growing season, defined as LAI > 0.5 (Lombardozzi et al., 2012), and reset with leaf shed. A leaf-turnover O₃ decay rate is included so that the accumulated O₃ damage did not accrue beyond the average leaf lifetime for evergreen plants.

2.1.3. Dry Deposition and Biogenic Emission Models Coupled With the Noah-MP Dynamic Vegetation Module

In the original WRF/Chem model, the resistance-in-series dry deposition scheme described in Wesely (2007) is used to calculate the gaseous dry deposition velocity (v_d):

$$v_d = (R_a + R_b + R_c)^{-1} \quad (6)$$

where R_a is the aerodynamic resistance; R_b is the laminar layer resistance; R_c is the surface resistance (Equation 7).

$$\frac{1}{R_c} = \frac{1}{R_s + R_m} + \frac{1}{R_{lu}} + \frac{1}{R_{cl}} + \frac{1}{R_g} \quad (7)$$

where R_s is the canopy stomatal resistance; R_m is the mesophyll resistance; R_{lu} is the skin resistance; R_{cl} is the lower canopy resistance; R_g is the ground resistance.

In the Wesely (2007) dry deposition scheme, the canopy stomatal resistance is calculated using an empirical algorithm (Equation 8):

$$R_s = r_m \times \left(1 + (200 \times (G + 0.1)^{-1})^2\right) \times (400 \times (T_s \times (40 - T_s))^{-1}) \times \frac{D_{H_2O}}{D_{O_3}} \quad (8)$$

where G is the solar radiation; T_s is the surface air temperature; r_m is the minimum stomatal conductance that is dependent on vegetation type and season; D_{H_2O} and D_{O_3} are the molecular diffusivity for vapor and ozone, respectively.

Instead, in this study we coupled the dry deposition scheme with the dynamic vegetation module in Noah-MP. The leaf-scale stomatal resistance (r_s) calculated from the Ball-Berry model (Equation 3) (Calatayud et al., 2007; Fiscus et al., 2005) and the dynamic LAI (Equation 2) are integrated through the canopy height to derive the canopy-scale stomatal resistance used for the calculation of gas dry deposition velocity.

$$\frac{1}{R_s} = \frac{f_{\text{sun}} \times \text{LAI}}{r_s^{\text{sun}}} + \frac{(1 - f_{\text{sun}}) \times \text{LAI}}{r_s^{\text{sha}}} \quad (9)$$

where f_{sun} is the sunlit fraction of leaf; r_s^{sun} and r_s^{sha} are the leaf-scale stomatal resistance for sunlit leaf and shaded leaf, respectively.

Biogenic volatile organic compound (BVOC) emissions from vegetation are calculated online using the Model of Emissions of Gases and Aerosols from Nature (MEGAN) version 2.04 (Guenther et al., 2006) in consideration of the impacts of plant type, environmental weather and leaf area (Equation 10).

$$E_{\text{BVOC}} = \text{EF}_{\text{BVOC}} \times \gamma_T \times \gamma_P \times \gamma_{\text{LAI}} \times \gamma_{\text{age}} \times \gamma_{\text{SM}} \\ \gamma_{\text{LAI}} = 0.49 \times \text{LAI} / \sqrt{1 + 0.2 \times \text{LAI}^2} \quad (10)$$

Table 1
The WRF/Chem-Noah-MP Model Scenarios

Simulation scenarios	Ozone damage to vegetation	MEGAN biogenic emission	Dry deposition velocity (v_d)	Ozone response parameters	Description
Dyn	Turned off	Fixed MODIS LAI as input to calculate γ_{LAI}	Empirical algorithm of canopy stomatal resistance in Wesely (2007) to calculate v_d	Lombardozzi et al. (2013)	To show the isolated impacts of ozone-vegetation coupling on meteorology and their chemical feedbacks.
Dyn-O ₃	Turned on				
DynBio	Turned off	Dynamic LAI calculated from Noah-MP to calculate γ_{LAI}	Empirical algorithm of canopy stomatal resistance in Wesely (2007) to calculate v_d		To show the impacts of ozone-vegetation coupling through meteorological and biogenic emission changes.
DynBio-O ₃	Turned on				
DynBioDry	Turned off	Dynamic LAI calculated from Noah-MP to calculate γ_{LAI}	Canopy stomatal resistance calculated from Noah-MP to calculate v_d		To show the combined impacts of ozone-vegetation coupling on air quality through meteorological and biogeochemical feedbacks.
DynBioDry-O ₃	Turned on				
DynBioDry_Sen-O ₃	Turned on	Same as DynBioDry-O ₃	Same as DynBioDry-O ₃	Lombardozzi et al. (2012)	To show the impacts of uncertainty in ozone response parameters on the model results.

where E_{BVOC} is the BVOC emission under real environmental conditions ($\text{mol km}^{-2} \text{ hr}^{-1}$); EF_{BVOC} is the canopy-scale emission factor under standard environmental conditions ($\text{mol km}^{-2} \text{ hr}^{-1}$); γ_T , γ_P , γ_{LAI} , γ_{age} , and γ_{SM} are a series of activity factors representing the impacts of ambient temperature, photosynthetically active radiation, LAI, leaf age and soil moisture on BVOC emissions, respectively.

By default, the global LAI data set derived from Moderate Resolution Imaging Spectroradiometer (MODIS) onboard the Terra and Aqua satellites (available at <https://modis.gsfc.nasa.gov>) are incorporated into MEGAN to calculate the γ_{LAI} factor (M. Li, Liu, et al., 2017; Li, Wang, et al., 2017). In this study, we couple the MEGAN biogenic emission model with the dynamic vegetation module, using the dynamic LAI calculated from Noah-MP (Equation 2) as input into MEGAN to estimate γ_{LAI} .

2.2. Simulation Experiments

We focus on the year 2017 that saw high ozone concentrations in China. The maximum daily 8-hr average (MDA8) O₃ concentrations in 2017 exceed the 2nd limit of National Ambient Air Quality Standard (200 $\mu\text{g m}^{-3}$) in 65% of the 74 major cities and ozone acts as the primary air pollutant in 43% of the pollution days (Bulletin, 2013–2017). The simulation lasts from December 2016 to December 2017, and the first 1-month is considered as spin-up and is excluded from the analysis. The 6-hr, $1^\circ \times 1^\circ$ National Centers for Environmental Prediction Final (NCEP/FNL) analysis data derived from the Global Data Assimilation System are regularly input for the model initial and lateral boundary meteorological conditions. Forcing CO₂ concentration used in the Noah-MP model is fixed at 380 ppm in all experiments, equal to the global averaged CO₂ mole fraction (Blunden & Arndt, 2014).

Three pairs of sensitivity simulations (denoted as Dyn vs. Dyn-O₃, DynBio vs. DynBio-O₃, and DynBioDry vs. DynBioDry-O₃ with the ozone-vegetation damages turned off and on separately) are designed to distinguish the meteorological and bio-geochemical feedbacks of ozone-vegetation coupling on air quality. In the Dyn and Dyn-O₃ scenarios, both the dry deposition and biogenic emission models are decoupled from the dynamic vegetation simulation to show the isolated impacts of meteorological feedback on air quality from ozone-vegetation coupling. The DynBio and DynBio-O₃ simulations are performed with the biogenic emission module coupled with dynamic vegetation simulation only to show the impacts of ozone-vegetation coupling on regional air quality through the modified meteorology and biogenic emission. In the DynBioDry and DynBioDry-O₃, both the dry deposition and biogenic emission modules are coupled with the dynamic vegetation simulation to show the combined impacts of ozone-vegetation coupling on regional air quality through meteorological and bio-geochemical feedbacks. Additionally, the ozone damage functions represent the main uncertainty in the model. We conduct another numerical experiment that assumes a simple linear decline of the plant photosynthesis and stomatal conductance with CUO independent of plant type (Lombardozzi et al. (2012), namely “*Lom12*”; Table S1 in Supporting Information S1) to illustrate the potential impacts of parameter uncertainty on the model results. The experimental details are presented in Table 1.

Table 2
Statistical Evaluations of the Model Results With Ground and Satellite Observations in the DynBioDry-O₃ Simulation

Index ^a	Temperature (°C)	Relative humidity (%)	Wind speed (m s ⁻¹)	MDA8 O ₃ (μg m ⁻³)	NO ₂ (μg m ⁻³)	GPP (μg C m ⁻² s ⁻¹)	Photosynthesis rate (μg C m ⁻² s ⁻¹)	LAI (m ² m ⁻²)
R	0.99	0.89	0.49	0.91	0.94	0.99	0.94	0.87
MB	-1.24	0.85	1.09	23.03	-6.12	-4.06	5.58	0.07
RMSE	1.34	2.38	1.11	25.91	6.95	5.48	7.94	0.36
NMB	-0.09	0.01	0.42	0.25	-0.19	-0.13	0.26	0.05

^aR: correlation coefficient; MB: mean bias; RMSE: root mean square error; NMB: normalized mean bias.

2.3. Observational Data

Surface weather data including 2 m air temperature, 2 m relative humidity and 10 m wind speed at 1-hr temporal resolution from 186 land-based automatic stations in China (Figure 1a) are collected for the model meteorological validation. These data are archived at the U. S. National Climatic Data Center (NCDC) (Smith et al., 2011). Hourly data of surface O₃ and nitrogen dioxide (NO₂) concentrations at the national air quality monitoring network covering more than 1,500 sites in 454 cities of China (Figure 1a) are used for the model chemical validation. The data are reported by Chinese National Environmental Monitoring Center (CNEMC, 2023).

Additionally, the MODIS global terrestrial GPP and photosynthesis rate data set at 1 km resolution (Running et al., 2015), and the MODIS LAI product at 1 km resolution (Myneni et al., 2015) are used for the model validation of vegetation physiology. Previous studies have suggested that the MODIS sensor performs well in vegetation monitoring, which could reflect the seasonal variations and magnitudes with a deviation within 15% (Fensholt et al., 2004; Myneni et al., 2002).

3. Results and Discussions

3.1. Model Validation Against Ground and Satellite Observations

We systematically assess the WRF/Chem model performance in simulating the basic meteorological and chemical variables, as well as vegetation physiology for the DynBioDry-O₃ scenario (Table 2). Our findings indicate that the spatial distributions and magnitudes of near-surface temperature, relative humidity and wind speed are well reproduced by the WRF/Chem-Noah-MP model (Figure 2), with the spatial correlation coefficients of 0.99, 0.89 and 0.49, and mean biases (MB) of -1.24°C, 0.85% and 1.09 m s⁻¹, respectively at the domain average (Table 2). Regionally, the model usually generates cool biases in southwestern and northeastern China and warm biases in mid-eastern China within ±3°C. Similarly, the model overestimates atmospheric humidity in Southwestern China by 7.21%, while it is underestimated by about -1.74% to -4.26% in other regions. Besides, the model generally overestimates near-surface wind speed in most regions, especially in northwestern and northeastern China. The seasonal cycles of near-surface temperature, humidity and wind speed are also clearly captured by the model, though with slight model biases by -0.88°C for temperature, 1.58% for relative humidity and 0.91 m s⁻¹ for wind speed during the April–October season.

Comparisons with the 1-year observational data from more than 1,500 air quality sites in China (Figure 3) also show that the simulated MDA8 O₃ and NO₂ concentrations reasonably reproduce the spatial distributions of air pollutants but deviate from the observed average concentrations by 23.03 μg m⁻³ (25.32%) and -6.11 μg m⁻³ (-18.87%) on average, which satisfied the US Environmental Protection Agency recommended statistical metrics. Besides, the model also clearly simulates the high-value ozone areas with annual-averaged MDA8 O₃ more than 120 μg m⁻³ stretching from North China to the middle and lower reaches of Yangtze River. In terms of the seasonal variations, the model also captures the lower NO₂ concentration and the peak ozone concentration during the warm season (April–October), despite with a serious overestimation of O₃ by over 30% in some regions, possibly due to the uncertain emissions and coarse model resolution. The high simulated bias in summertime ozone concentration is a commonly acknowledged issue in Asia with global and regional models. For example, Gong et al. (2020) overestimated the summertime averaged ozone concentration by 29.3% globally, mainly resulting from the ozone overestimation in China. Using a fully coupled chemistry–carbon–climate global model, Yue et al. (2017) also pointed out that the model overestimated the annual average ozone concentration of China by >40% with comparison against observations from 188 urban sites.

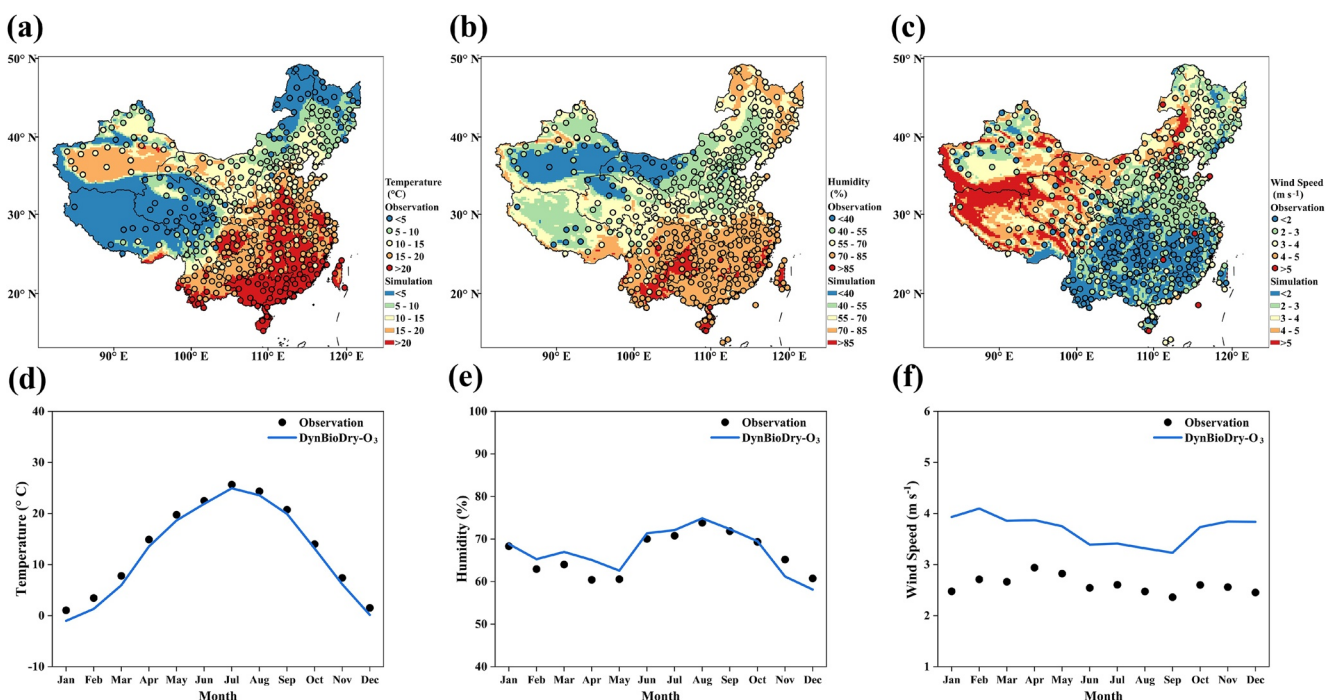


Figure 2. Comparisons of the (a–c) spatial distributions of annual averages and (d–f) monthly variations of near-surface temperature, relative humidity and wind speed from model simulation with ground observations in China.

Additionally, several MODIS products are interpolated to the model resolution to validate the simulated vegetation physiology parameters (Figure 4). Overall, the model reasonably simulates the spatial patterns and magnitudes for the terrestrial primary productivity and vegetation parameters against satellite observations, featured by high values in South China where forests dominate. The simulated photosynthesis rate, GPP and LAI show high spatial correlation coefficients ($R = 0.94, 0.99$ and 0.87) and low model-to-observation biases (MB of $5.58 \mu\text{g C m}^{-2} \text{s}^{-1}$, $-4.06 \mu\text{g C m}^{-2} \text{s}^{-1}$ and $-0.07 \text{m}^2 \text{m}^{-2}$, and normalized mean bias (NMB) of 26.02% , -12.61% and -5.66%) on the national scale (Table 2). Ma et al. (2017) evaluated the Noah-MP model against in-situ flux observations and also found that Noah-MP biased GPP by 40% over U. S. The simulations for terrestrial GPP and LAI also exhibit reasonable seasonality (e.g., a maximum in summer for vegetated areas) over China, but with clear underestimate of the peak values to some extent during May–October (Figure 4). The prognostic treatment of carbon cycle and LAI calculation in dynamic vegetation model is known to be problematic, with large uncertainties in the model parameterization, photosynthetic parameters and dynamic treatment of nitrogen (Bonan et al., 2011). Comparisons in several major regions of China (Figure S1 in Supporting Information S1) further show that the model deviates from satellite measurements within $\pm 30\%$ in most regions, except in North China Plain with substantial regional bias probably due to the absence of crop growth model in this study (Warrach-Sagi et al., 2022).

We also evaluated the potential model improvement attributed to the optimized WRF/Chem-Noah-MP model. The sensitivity simulations with/without the ozone-vegetation coupling indicate that the simulation of vegetation-related parameters is obviously improved in DynDryBio-O₃ compared with DynDryBio simulation (Figure 4). The model errors of photosynthesis, GPP and LAI compared with satellite observations are reduced by $14.93 \mu\text{g C m}^{-2} \text{s}^{-1}$ (57.54%), $3.0 \mu\text{g C m}^{-2} \text{s}^{-1}$ (7.14%) and $0.21 \text{m}^2 \text{m}^{-2}$ (10.80%) respectively during the plant-growing season after the inclusion of ozone-vegetation coupling. But in terms of the meteorological and chemical simulations, because the model accuracy is influenced by many complicated factors such as plenty of parameterizations and uncertainties in input data, the inclusion of ozone-vegetation coupling does not guarantee remarkable model improvement. For example, the model errors of surface temperature and relative humidity are reduced by 0.06°C (0.44%) and 0.41% (0.62%) while that of ozone slightly decreases in northeastern China by $0.27 \mu\text{g m}^{-3}$ (0.32%) in DynBioDry-O₃ compared to the baseline DynBioDry scenario (data not shown here). Otherwise the optimized gaseous dry deposition scheme coupled with Noah-MP dynamic vegetation module also provides improved simulation of ozone dry deposition velocity against field observations (Table 3), which will be discussed in detail in Section 3.3.

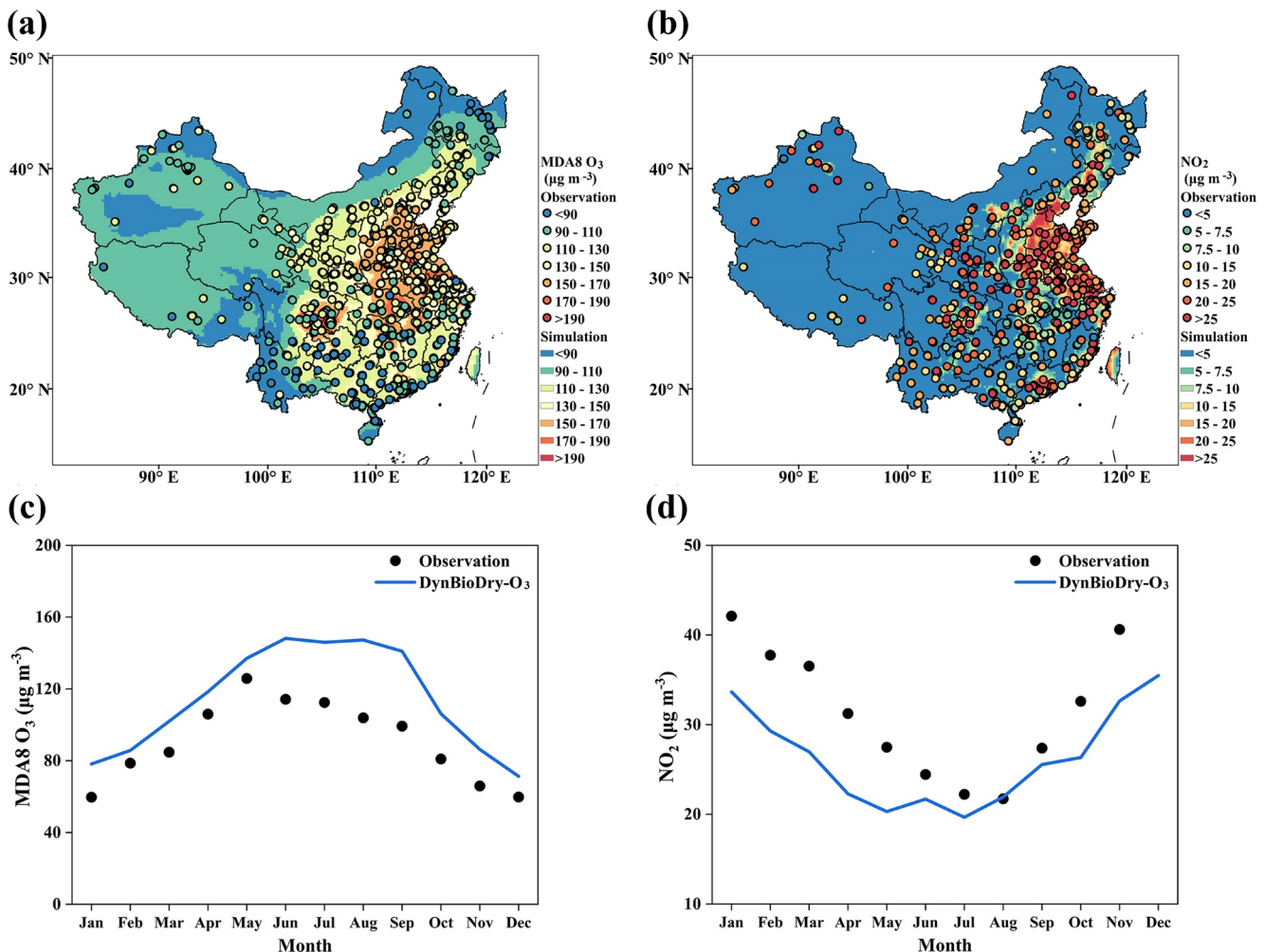


Figure 3. Comparisons of the (a–b) spatial distribution of the surface average MDA8 O₃ and NO₂ concentrations during the April–October warm season and (c–d) monthly variations of surface MDA8 O₃ and NO₂ concentrations from model simulation with ground observations in China.

3.2. Impacts of Ozone-Vegetation Coupling on Surface Heat Flux and Meteorology

Ozone-vegetation coupling may have significant impacts on regional water/heat flux between the land and atmosphere, which in turn causes complex climatic feedbacks. Here we select two simulations with/without ozone-vegetation coupling (DynBioDry-O₃ and DynBioDry scenarios) to determine the effects of ozone-vegetation damage on regional heat flux and meteorology (Figures 5 and 6) and their seasonal variations (Figure S3 in Supporting Information S1). During the growing season, the accumulated ozone uptake has high values ranging between 8.63 and 13.59 mmol m⁻² in South, East, and Central China with dense vegetation coverage (Figure S2 in Supporting Information S1). The overall CUO distribution does not exactly follow that of surface ozone concentration because the leaf ozone uptake also depends on the vegetation stomatal conductance. The simulated CUO values are comparable with the global study by Lombardozzi et al. (2015) in terms of both magnitude and spatial distribution.

In accordance with the CUO pattern, the O₃-damaged plant photosynthesis rate and stomatal conductance are reduced by –29.94% and –17.46% averagely over China at the canopy-scale (Figure 5). The maximum reductions are found in the low-middle latitude regions south of 30°N in China featured by both high surface ozone levels and abundant vegetation coverage, for example, East and South China with more than 30% decline of photosynthesis and stomatal conductance during the summer season. As expected, the elevated ozone damages plant photosynthesis and consequently affects the terrestrial primary productivity. After incorporating the ozone-vegetation coupling into WRF/Chem-Noah-MP model, it is estimated that the surface O₃ exposure decreases annual GPP and net primary productivity (NPP) in China by –10.67 µg C m⁻² s⁻¹ (–29.23%) and –5.49 µg C m⁻² s⁻¹ (–28.47%),

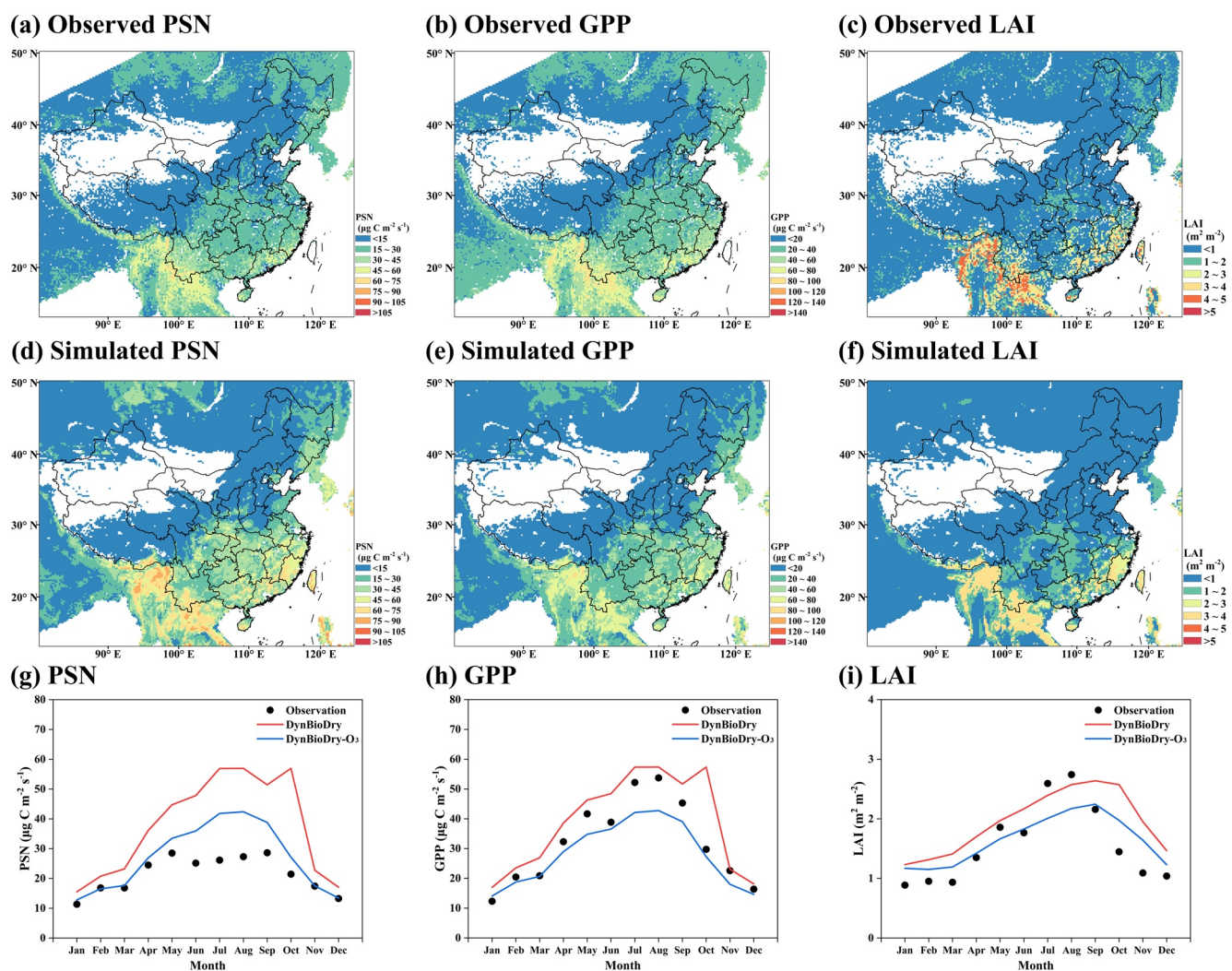


Figure 4. Comparisons of the (a–f) spatial distributions of annual averages and (g–i) monthly variations of photosynthesis rate (left panels), gross primary productivity (middle panels) and leaf area index (right panels) from model simulation with MODIS satellite data in China.

respectively. The ozone damage to LAI generally follows that of GPP reductions but the response signal is weaker, with an average LAI decrease of $-0.31 \text{ m}^2 \text{ m}^{-2}$ (-17.41%) in China. Locally, the ozone damages to vegetation LAI reach as high as $-0.36 \text{ m}^2 \text{ m}^{-2}$ (-15.07%) in East China. These values estimated using Noah-MP

Table 3
Comparisons of Simulated Ozone Dry Deposition Velocity With Field Observations From Previous Studies

Location	Underlying surface	Period	Dry deposition velocity (cm s^{-1})				References
			Field observations	DynBioDry-O ₃	DynBioDry	DynBio	
Nanjing (34°N, 113°E)	Cropland	10 March–10 May 2018	0.38	0.39	0.41	0.48	Wei (2019)
		16 July–14 September 2018	0.42	0.41	0.43	0.46	
Nanjing (34°N, 113°E)	Cropland	26 July–26 September 2018	0.41	0.40	0.40	0.45	Guan (2019)
Nanjing (34°N, 113°E)	Cropland	16 March–30 May 2016	0.39	0.47	0.41	0.48	Xu et al. (2018)
Nanjing (34°N, 113°E)	Bare soil	25 September–20 November 2015	0.20	0.35	0.36	0.35	Huang et al. (2016)
Yucheng (36°N, 116°E)	Cropland	7 March–7 June 2012	0.28	0.39	0.39	0.49	Zhu et al. (2015)
Zhaqing (23°N, 116°E)	Forest	21 August–21 November 2019	0.34	0.46	0.49	0.47	Cao et al. (2022)
Beijing (40°N, 116°E)	Grass	23 September–13 October 2007	0.55	0.29	0.30	0.31	Pan et al. (2010)

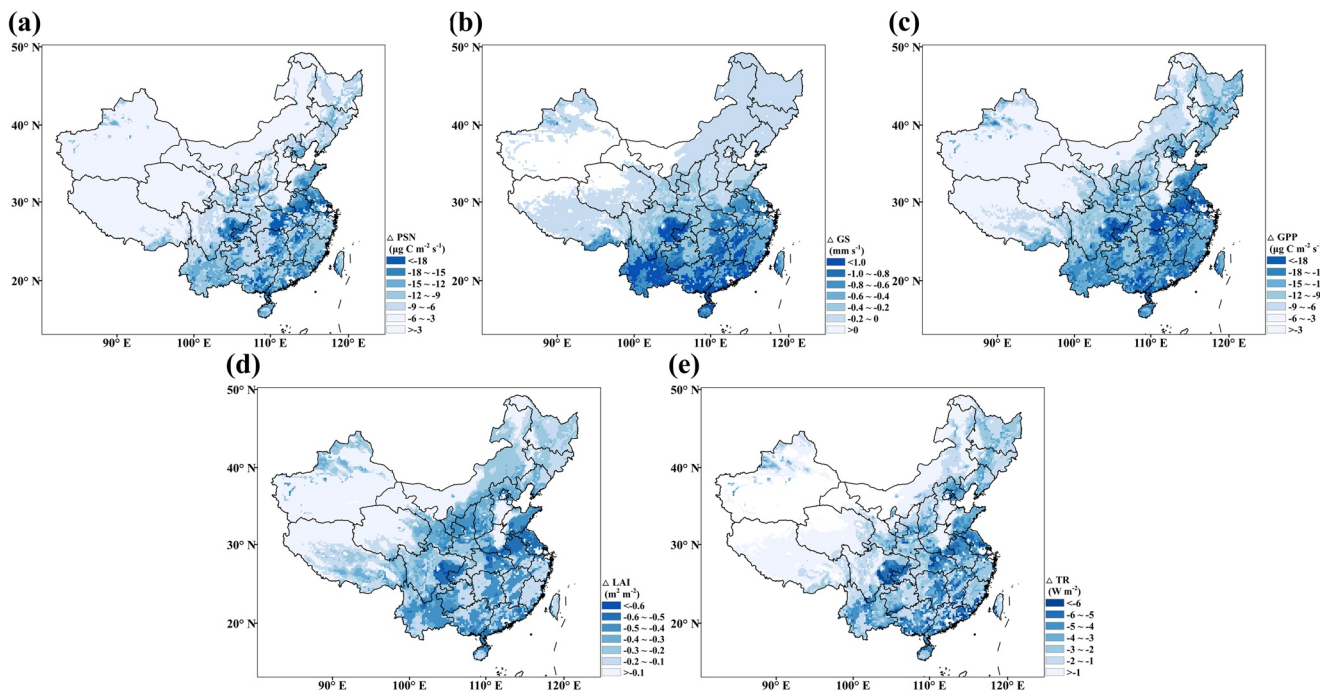


Figure 5. Annual averaged changes of (a) vegetation photosynthesis rate, (b) stomatal conductance, (c) gross primary productivity, (d) leaf area index and (e) transpiration rate due to ozone-vegetation damage.

in this study are consistent with previous estimates ranging from 5% to 50% for GPP decrease and 10%–30% for NPP decrease over China and other regions globally with different land models and ozone-vegetation parameterizations (Table S2 in Supporting Information S1) (Ainsworth et al., 2012; B. Felzer et al., 2005; J. Li et al., 2016; Lombardozzi et al., 2012, 2013, 2015; Ren et al., 2011; Sadiq et al., 2017; Super et al., 2015; Xie et al., 2019; B.

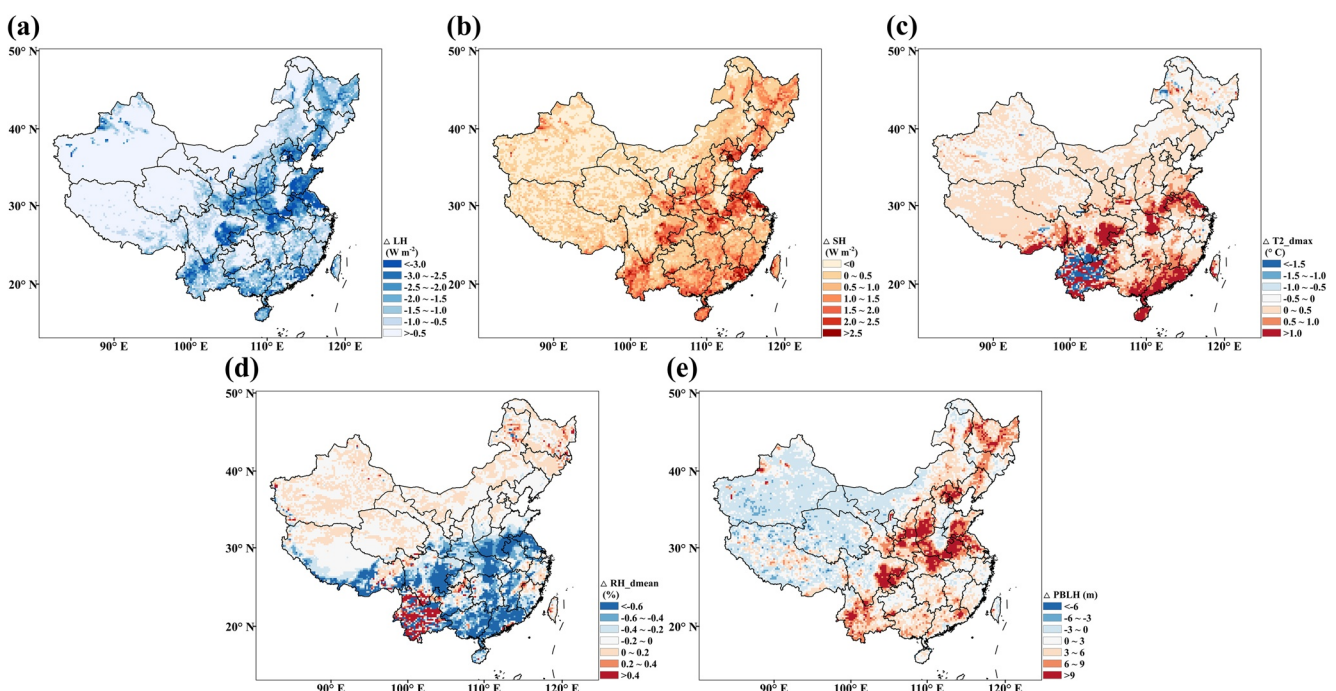


Figure 6. Annual averaged changes of surface (a) latent heat flux, (b) sensible heat flux, (c) near-surface daily maximum temperature, (d) daytime-average humidity and (e) boundary layer height due to ozone-vegetation coupling.

J. Yue et al., 2017). The different empirical parameterizations used to represent the plant responses to ozone may explain the large discrepancies in these model estimates.

The ozone-induced stomatal behavior and vegetation physiology changes might lead to alterations in plant transpiration and therefore surface heat flux. The plant TR in Noah-MP is estimated using the dynamic vegetation LAI and stomatal conductance calculated from the Farquhar/Ball-Berry model. Compared to the control simulation, the vegetation TR in DynBioDry-O₃ scenario decrease in most regions of China because of the stomatal injury due to O₃ by -17.47% nationally, which is a more obvious change compared with the decrease (2%–6%) of previous global estimates (Lombardozzi et al., 2015; Sadiq et al., 2017). The largest declines of TR are simulated in South China (-16.57%) and East China (-18.66%). The suppressive plant transpiration further causes the latent heat exchange to decrease by -2.20% and the sensible heat flux to increase by -1.68% on annual-average across China. Similar with that of TR, most affected regions are found in South and East China (Figure 5). The O₃-induced reductions in stomatal conductance inhibit plant transpiration and weaken the process of surface dissipating heat, leading to warmer and drier air, as clearly shown in Figure 6. The daytime average atmospheric humidity decreases in response to the suppressed plant transpiration in a range of regions, but those changes are moderate within -0.6% (up to -0.74% in summer) compared to the control simulation. Similarly, the ozone exposure increases daily maximum temperature by a magnitude of up to 0.16°C in summer nationally, which further regulate the atmospheric boundary layer development (an increase of roughly 8.45 m in summer). Particularly, stronger inhibitions of O₃ on near-surface meteorology are found for the northern to northeastern China regions, for example, with the largest increase of temperature by 0.07–0.24°C in summer. The changes of model heat fluxes and near-surface climate are consistent with field experiments (Bernacchi et al., 2011) and offline model studies (Lombardozzi et al., 2012, 2015; Sadiq et al., 2017) (as shown in Table S2 in Supporting Information S1), who presented a plausible mechanism of ozone damage to hydrologic cycle by changing transpiration rates on regional and global scales.

Many previous regional or global studies (Sitch et al., 2007; Super et al., 2015; Xie et al., 2019; Yue et al., 2017) assume that photosynthesis declines linearly with CUO, although the plant-specific response parameters used in this study following Lombardozzi et al. (2013) suggest that this assumption is not accurate. Lombardozzi et al. (2013) reported an overall 21% decrease in leaf-level photosynthesis rate and 11% decrease in leaf-level stomatal conductance from a meta-analysis of 750 independent measurements and represented the most comprehensive database available to date. Although Lombardozzi et al. (2013) observed a similar decrease in photosynthesis, the lack of correlation between photosynthesis and CUO when generalizing across plant species was different from the strong negative correlations used in many previous models. We further tested the impacts of parameter uncertainty on the model results assuming a linear decline of photosynthesis and stomatal conductance with CUO (Lombardozzi et al., 2012) (Table S1 in Supporting Information S1) in the DynBioDry_Sen-O₃ experiment (as shown in Figure 7). Overall, the simulated spatial distributions for the ozone-coupling effects on vegetation phenology and meteorological elements are similar for the two scenarios with different response parameters. As for the impacts of ozone-vegetation coupling on vegetation-related parameters, the two scenarios with different response parameters differed by roughly 2.06 µg C m⁻² s⁻¹ (12.36%), 2.16 µg C m⁻² s⁻¹ (12.74%) and 0.06 m² m⁻² (14.00%) for photosynthesis rate, GPP and LAI, respectively on the national scale during the plant-growing season. Compared with the DynBioDry-O₃ scenario, the application of the “*Lom12*” linear-response scheme seems to generate roughly ~20% larger ozone-induced temperature increase and humidity decrease in summer than the “*Lom13*” response scheme.

3.3. Feedbacks of Ozone-Vegetation Coupling on Surface Ozone Air Quality

Foliar stomatal uptake of ozone could further induce a series of meteorological and biogeochemical feedbacks on ozone air quality itself (Gong et al., 2020; Sadiq et al., 2017). We implement a series of sensitivity experiments (Table 1) to explain the feedbacks between ozone-vegetation coupling and regional air quality. Figure 8 shows the changes in surface ozone concentrations attributed to the altered regional meteorology (i.e., “meteorological feedback”), and biogenic emissions and dry deposition (together referred to as “biochemical feedback”) due to the ozone-vegetation coupling. The ozone-induced meteorological changes may affect regional air quality through directly impacting the chemical production of ozone and indirectly modifying the biogenic emissions. The meteorological changes alone contribute about 0.49 µg m⁻³ (0.85 µg m⁻³ in summer) increase of surface ozone concentration on the national scale (i.e., Dyn and Dyn-O₃ scenarios) through the aforementioned meteorological

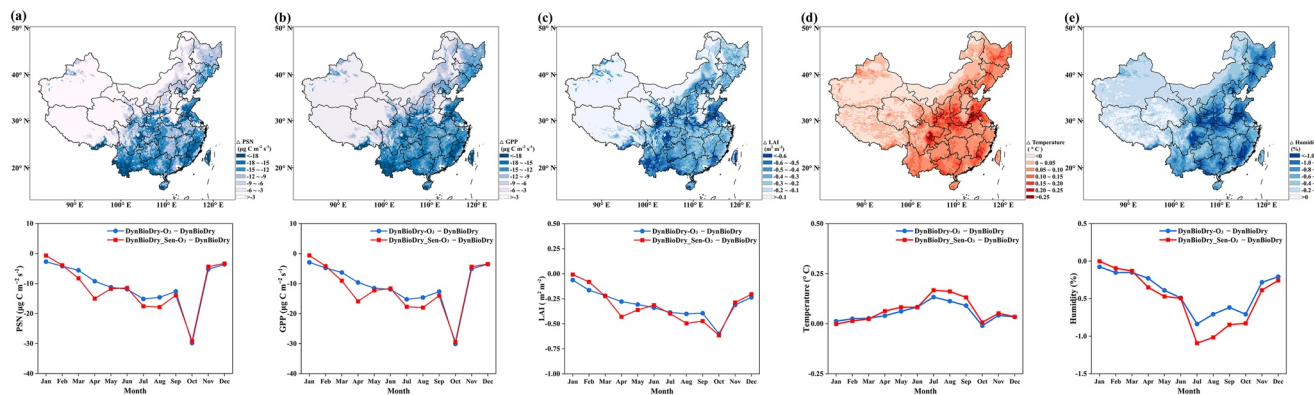
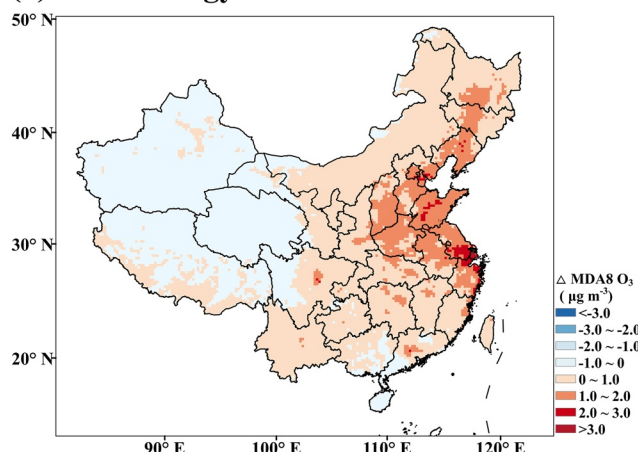


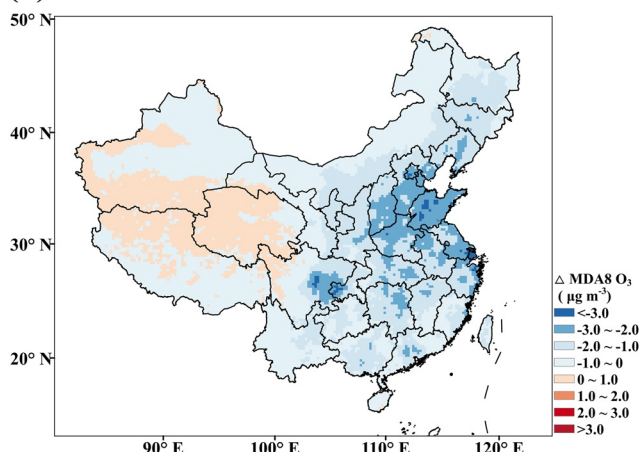
Figure 7. Changes of the spatial distributions (upper panels) and monthly variations (bottom panels) of (a) vegetation photosynthesis rate, (b) gross primary productivity, (c) leaf area index, (d) near-surface temperature and (e) relative humidity due to the ozone-vegetation coupling simulated in the DynBioDry_Sen-O₃ and DynBioDry-O₃ scenarios with different response parameters.

changes induced by ozone-vegetation coupling, such as higher temperature and lower humidity that facilitate the chemical production of ozone, as well as higher biogenic emission under warmer ambient condition that indirectly contribute to higher ozone levels. Furthermore, the maxima increase of near-surface ozone generally

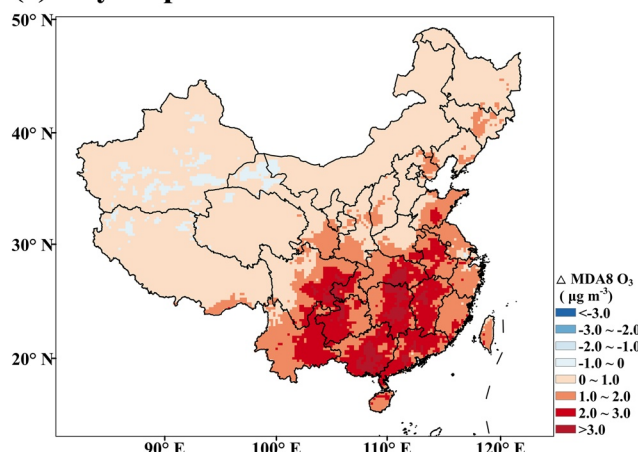
(a) Meteorology



(b) BVOCs



(c) Dry-Deposition



(d) All mechanisms

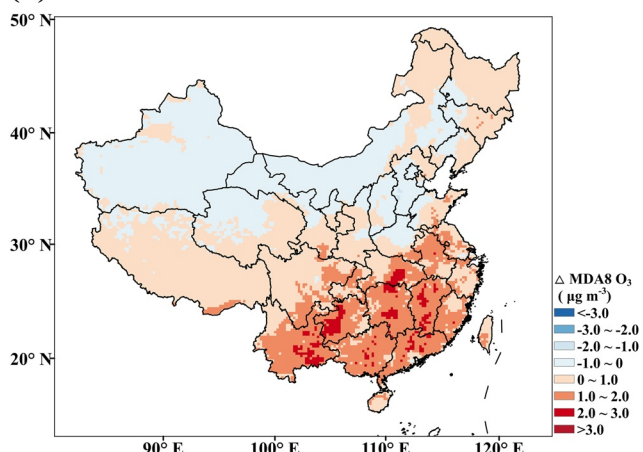


Figure 8. Annual averaged changes of surface MDA8 O₃ concentrations through three different mechanisms. (a) Meteorological feedback (Dyn-O₃ vs. Dyn), (b) altered biogenic VOC_s emission (DynBio-O₃ vs. DynBio), (c) altered ozone dry deposition, (d) total influence ($\Delta\text{O}_3 = \text{DynBioDry-O}_3 - \text{DynBioDry}$).

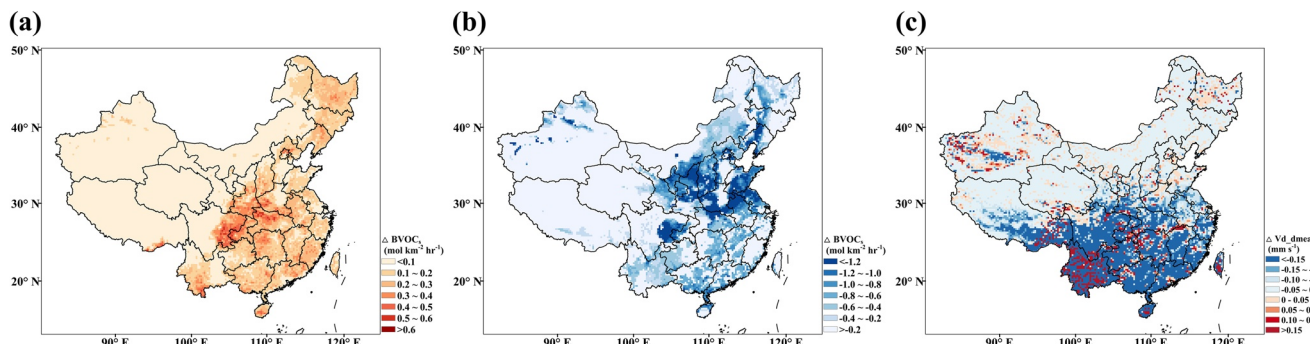


Figure 9. Annual averaged changes of Biogenic volatile organic compound emissions resulting from (a) meteorology changes and (b) suppressed photosynthesis rate and leaf area index. (c) Annual averaged changes of ozone dry-deposition velocity due to ozone-vegetation coupling.

accompanies with the areas featured by clear increase of surface temperature and decrease of relative humidity, as it appears at a magnitude of about $1.28 \mu\text{g m}^{-3}$ over East China where humidity and temperature are simulated to change most, which are comparable to the results modeled by Gong et al. (2020).

In addition to the meteorological feedback, the changes in gaseous dry deposition and biogenic emissions due to the suppressed photosynthesis and LAI may be the other two major biogeochemical pathways modulating the near-surface ozone air quality. Isoprene and monoterpene are estimated to be the most significant BVOC species in China, totally accounting for 74.62% of the national BVOC emission in our model results and is comparable to the estimation (59%–69%) by Li and Xie (2014). Besides, the magnitude for the annual BVOC emission ($21.09 \text{Tg C yr}^{-1}$) in this study is also similar with the recent estimation by K. Wu et al. (2020) (24Tg yr^{-1} in 2017), confirming the reliability of the model results of MEGAN estimation. In addition to the ambient weather conditions, the BVOC emitted by plants might also be influenced by the suppressed vegetation photosynthesis rate and resultantly lower LAI due to ozone exposure. As shown in Figure 9, LAI is a key driving factor of BVOC emission and the strong decline of LAI in China due to the ozone damage to photosynthesis rate result in a clear decrease of the BVOC emissions mainly in Central and South China (averagely $-0.71 \text{ mol km}^{-2} \text{ hr}^{-1}$ annually) with high vegetation coverage. As the main precursor for ozone, the BVOC emission decrease induce a changes of surface ozone levels in central ($-1.65 \mu\text{g m}^{-3}$) and northern China ($-1.20 \mu\text{g m}^{-3}$). This phenomenon results from the fact that northern China is mainly dominated by VOC-limited regimes where higher VOC emission benefits ozone formation, while in southern China with already abundant VOC emissions the decreased biogenic emissions have little effect on ozone formation (K. Wu et al., 2020). But with fully coupled online WRF/Chem-MEGAN model, it's difficult to isolate the two counterpart influences of BVOC emissions due to the ozone-vegetation coupling. We note that the decreased annual-average BVOC emissions ($-0.87 \text{ mol km}^{-2} \text{ hr}^{-1}$ nationally) due to the suppressed photosynthesis rate and LAI far surpass the increased BVOC emission ($0.17 \text{ mol km}^{-2} \text{ hr}^{-1}$ nationally) due to higher ambient temperature with ozone-vegetation coupling, which consequently constitutes negative feedback on surface ozone levels.

Besides, dry deposition is one of the most significant sinks for surface ozone particularly over the vegetated regions. Table 3 compares the ozone dry deposition velocity calculated from the optimized and original dry deposition algorithms against field observations at specific locations and periods in China from previous studies. It is noted that the misrepresentation of canopy stomatal resistance in the original Wesely (2007) dry deposition algorithm of DynBio simulation may seriously overestimate the ozone dry deposition velocity at most of the selected sites by about $0.04\text{--}0.21 \text{ cm s}^{-1}$ (Table 3). By contrast, the optimized dry deposition scheme that is coupled with dynamic vegetation module agrees much better with field observations, with the model errors of ozone dry deposition velocity reduced by $0.03\text{--}0.07 \text{ cm s}^{-1}$ in DynDryBio and $0.01\text{--}0.03 \text{ cm s}^{-1}$ in DynDryBio-O₃. Besides, the original dry deposition algorithm of WRF/Chem in DynBio may worsen the summertime ozone overestimation, which is further reduced by roughly $0.38 \mu\text{g m}^{-3}$ (1.04%) due to the optimized dry deposition module in the DynBioDry model (data not shown here). Val Martin et al. (2014) and Clifton et al. (2020) also introduced dynamic dry deposition scheme in the regional climate-chemistry model and found significantly improved simulation of ozone in vegetated regions. But our results still seem to be seriously positively biased at the Yucheng site and negatively biased at the Beijing site with deviations nearly $\pm 40\%$. The two sites are both located in North China with underlaying surface covered by cropland and grass, and the large biases may be partly attributed to the

missing of crop growth model in the simulation. Furthermore, our study suggests that the ozone dry deposition is reduced across China following the ozone-induced increase in canopy-level stomatal resistance (Figure 9), resulting in an increase of surface ozone levels (averagely $1.18 \mu\text{g m}^{-3}$). For example, the declined LAI ($\sim 14\%$) and stomatal conductance ($\sim 20\%$) in southern China combine to reduce the daytime-average ozone dry deposition velocity by -3.03% (Figure 9), contributing to a maximum ozone increase of $2.34 \mu\text{g m}^{-3}$. Most of the near-surface ozone changes due to the ozone-vegetation coupling are driven by the declined ozone dry deposition, especially in the densely vegetated southern regions with about $66\%-69\%$ attribution. Previous global study by Sadiq et al. (2017) also supports our opinion which reported that $40\%-100\%$ of the ozone increase produced by the ozone-vegetation coupling could be attributed to the ozone damage to dry deposition and TR.

Overall, the ozone-vegetation coupling constitutes a complex feedback loop that ultimately modify the near-surface ozone level by about $-0.12\sim 1.40 \mu\text{g m}^{-3}$ on average nationally ($-0.74\sim 1.12 \mu\text{g m}^{-3}$ in summer). Therein, the lower ozone dry deposition velocity due to the increased canopy-level stomatal resistance ($1.18 \mu\text{g m}^{-3}$ averagely) and the lower BVOC emission due to the suppressed photosynthesis rate and LAI ($-1.07 \mu\text{g m}^{-3}$ averagely) seem to be the dominant contributors to the surface ozone changes in China. Despite that the simulated changes in surface ozone levels due to ozone-vegetation coupling are small compared to the possible impact of climate and land cover changes on surface ozone, which are in the range of $2.1\sim 21.4 \mu\text{g m}^{-3}$ (K. Li et al., 2020; Tai et al., 2013; Val Martin et al., 2015), the inclusion of ozone damage in a coupled climate-chemistry-biosphere framework can have a potentially significant impact on surface ozone simulations.

4. Conclusion

The leaf stomatal uptake of ozone reduces both vegetation photosynthetic rate and stomatal conductance, which can induce a cascade of effects that ultimately modulate climate, carbon cycle and also feedback onto ozone air quality itself. In this study, the Noah-MP land surface model with dynamic vegetation module in WRF/Chem is modified to include the impacts of chronic ozone exposure on plant photosynthesis rate and stomatal conductance. Compared with ground observations and satellite data, the optimized WRF/Chem model could reasonably reproduce the spatial patterns of near-surface meteorology, ozone air pollutants and vegetation physiology, with a spatial correlation coefficient of more than 0.9 and NMB ranging from -0.19 to 0.42 . Our results also indicate that the incorporation of vegetation-ozone interactions into the online WRF/Chem coupled with the Noah-MP dynamic vegetation module can moderately improve the model simulations of vegetation physiology (e.g., a reduction of model error by $18\%-32\%$) and ozone dry deposition velocity. The effects of ozone exposure on regional water/heat flux and climate are further investigated. The elevated O_3 leads to -29.23% and -17.41% decreases of annual terrestrial GPP and LAI on the national scale, respectively. The O_3 -damaged stomatal conductance weakens plant transpiration and modifies the surface heat flux, which induces the daytime atmospheric humidity and maximum temperature to be altered by as high as -0.74% and 0.16°C in summer. Furthermore, the ozone-vegetation coupling induces a complex feedback loop on ozone air quality itself. Totally, the ozone-vegetation coupling act to cause an ozone change by $-1.00\sim 1.40 \mu\text{g m}^{-3}$ nationally. Among all the feedback paths, the decreased ozone dry deposition velocity due to the increased canopy-level stomatal resistance ($1.18 \mu\text{g m}^{-3}$) and the lower BVOC emission due to the suppressed photosynthesis rate and LAI ($-1.07 \mu\text{g m}^{-3}$) seem to be the dominant contributors to surface ozone changes in China. Our results highlight the necessity of including the ozone-vegetation interactions in regional models to get a complete understanding and reliable predictions of regional climate and air quality.

There remains considerable uncertainty associated with the parameterization of ozone-vegetation damage. The O_3 response function used in this study is based on three generic plant functional types (deciduous, evergreen and grass/crop; see Lombardozzi et al. (2013)), and does not include specific crop and tree responses. Additionally, the O_3 -response functions are primarily based on controlled chamber experiments under high O_3 concentrations (Lombardozzi et al., 2013), which may differ from the real atmospheric conditions. The model results could possibly be improved with more detailed plant-type-specific O_3 -damage parameterization, including better estimates of plant vulnerability to ozone that will refine the ozone uptake thresholds (Lombardozzi et al., 2015). Additionally, current large mechanistic uncertainties in the role of anthropogenic nitrogen (N) deposition to China's land carbon uptake (Tian et al., 2011; Xiao et al., 2015) have prohibited the inclusion of dynamic carbon-nitrogen coupling in the Earth system model. Previous studies have suggested that inclusion of nitrogen fertilization can relieve or offset damages by O_3 , especially for N-limited forests (Ollinger et al., 2002), which is not considered in this study.

Many climate-chemistry-biosphere modeling studies have also demonstrated the importance of the coevolution of climate, land cover and terrestrial ecosystems in air quality simulations and predictions (Pacifico et al., 2015; Tai et al., 2013; Wu et al., 2012). Particularly, estimations from a range of RCP emission scenarios support that the O₃ concentrations will increase by 25% over the next 30–50 years in many regions of the world (Cooper et al., 2010; Wild et al., 2012), exacerbating the negative impacts of O₃ on plants and climate. This study may provide a new idea for better understanding the interactions between climate, atmospheric chemistry and ecosystem under the background of global changes.

Data Availability Statement

The WRF/Chem model (Skamarock et al., 2019) code is available at <https://github.com/wrf-model/WRF>. The NCEP FNL data are accessible at the National Center for Atmospheric Research (NCAR) Research Data Archive (RDA, 2023; <http://rda.ucar.edu/datasets/ds083.2/>). The MEIC anthropogenic emission inventory is available at <http://meicmodel.org.cn/> (Li, Liu, et al., 2017; Li, Wang, et al., 2017; Zheng et al., 2018). The air pollutants data are provided by Chinese National Environmental Monitoring Center (CNEMC, 2023). The surface weather data are accessible at the Integrated Surface Database (NOAA, 2001; <ftp://ftp.ncdc.noaa.gov/pub/data/noaa/>). The MODIS land products are provided by Land Process Distributed Active Archive Center (LP-DAAC; https://lpdaac.usgs.gov/dataset_discovery/modis/modis_products_table/) (Myeni et al., 2015; Running et al., 2015). Main observational data and WRF/Chem code used in this study is archived on Zenodo (Jin and Li., 2023).

Acknowledgments

This study is funded by the National Key Basic Research Development Program of China (2022YFC3701105 and 2020YFA0607802), the National Natural Science Foundation of China (41975153, 42275100, and 42077192), the Research Funds for the Frontiers Science Center for Critical Earth Material Cycling, Nanjing University (14380189), and the Post-graduate Research & Practice Innovation Program of Jiangsu Province.

References

- Ainsworth, E. A., Yendrek, C. R., Sitch, S., Collins, W. J., & Emberson, L. D. (2012). The effects of tropospheric ozone on net primary productivity and implications for climate change. *Annual Review of Plant Biology*, 63(1), 637–661. <https://doi.org/10.1146/annurev-arplant-042110-103829>
- Avise, J., Chen, J., Lamb, B., Wiedinmyer, C., Guenther, A., Salathé, E., & Mass, C. (2009). Attribution of projected changes in summertime US ozone and PM 2.5 concentrations to global changes. *Atmospheric Chemistry and Physics*, 9(4), 1111–1124. <https://doi.org/10.5194/acp-9-1111-2009>
- Ball, J. T., Woodrow, I. E., & Berry, J. A. (1987). A model predicting stomatal conductance and its contribution to the control of photosynthesis under different environmental conditions, In *Progress in photosynthesis research* (pp. 221–224). Springer. https://doi.org/10.1007/978-94-017-0519-6_48
- Barlage, M., Tewari, M., Chen, F., Miguez-Macho, G., Yang, Z. L., & Niu, G. Y. (2015). The effect of groundwater interaction in North American regional climate simulations with WRF/Noah-MP. *Climatic Change*, 129(3–4), 485–498. <https://doi.org/10.1007/s10584-014-1308-8>
- Bernacchi, C. J., Leakey, A. D., Kimball, B. A., & Ort, D. R. (2011). Growth of soybean at future tropospheric ozone concentrations decreases canopy evapotranspiration and soil water depletion. *Environmental Pollution*, 159(6), 1464–1472. <https://doi.org/10.1016/j.envpol.2011.03.011>
- Blunden, J., & Arndt, D. S. (2014). Supplement: State of the climate in 2013 supplemental figures. *Bulletin of the American Meteorological Society*, 95(7), ES1–ES22. <https://doi.org/10.1175/2014amsstateoftheclimate.1>
- Bonan, G. B. (2008). Forests and climate change: Forcings, feedbacks, and the climate benefits of forests. *Science*, 320(5882), 1444–1449. <https://doi.org/10.1126/science.115121>
- Bonan, G. B., Lawrence, P. J., Oleson, K. W., Levis, S., Jung, M., Reichstein, M., et al. (2011). Improving canopy processes in the Community Land Model version 4 (CLM4) using global flux fields empirically inferred from FLUXNET data. *Journal of Geophysical Research*, 116(G2), G02014. <https://doi.org/10.1029/2010JG001593>
- Bulletin, C. E. S. (2013–2017). Chinese environmental statistical bulletin. In *Ministry of ecology and environment of the people's Republic of China*.
- Calatayud, V., Cerveró, J., & Sanz, M. J. (2007). Foliar, physiological and growth responses of four maple species exposed to ozone. *Water, Air, & Soil Pollution*, 185(1), 239–254. <https://doi.org/10.1007/s11270-007-9446-5>
- Cao, J., Chang, M., Pan, Y., Song, T., Liu, Z., Zhao, H., et al. (2022). Assessment and intercomparison of ozone dry deposition schemes over two ecosystems based on Noah-MP in China. *Atmospheric Environment*, 290, 119353. <https://doi.org/10.1016/j.atmosenv.2022.119353>
- Clifton, O., Paulot, F., Fiore, A., Horowitz, L., Correa, G., Baublitz, C., et al. (2020). Influence of dynamic ozone dry deposition on ozone pollution. *Journal of Geophysical Research: Atmospheres*, 125(8), e2020JD032398. <https://doi.org/10.1029/2020JD032398>
- CNEMC. (2023). China national environmental monitoring centre. [Dataset]. CNEMC. Retrieved from www.cnemc.cn/en/
- Collatz, G. J., Ball, J. T., Grivet, C., & Berry, J. A. (1991). Physiological and environmental regulation of stomatal conductance, photosynthesis and transpiration: A model that includes a laminar boundary layer. *Agricultural and Forest Meteorology*, 54(2–4), 107–136. [https://doi.org/10.1016/0168-1923\(91\)90002-8](https://doi.org/10.1016/0168-1923(91)90002-8)
- Cooper, O. R., Parrish, D., Stohl, A., Trainer, M., Nédélec, P., Thouret, V., et al. (2010). Increasing springtime ozone mixing ratios in the free troposphere over western North America. *Nature*, 463(7279), 344–348. <https://doi.org/10.1038/nature08708>
- Cuntz, M., Mai, J., Samaniego, L., Clark, M., Wulfmeyer, V., Branch, O., et al. (2016). The impact of standard and hard-coded parameters on the hydrologic fluxes in the Noah-MP land surface model. *Journal of Geophysical Research: Atmospheres*, 121(18), 10676–10700. <https://doi.org/10.1002/2016JD025097>
- Ek, M. B., Mitchell, K. E., Lin, Y., Rogers, E., Grunmann, P., Koren, V., et al. (2003). Implementation of Noah land surface model advances in the National Centers for Environmental Prediction operational mesoscale Eta model. *Journal of Geophysical Research*, 108(D22), 8851. <https://doi.org/10.1029/2002jd003296>
- Farquhar, G. D., von Caemmerer, S. V., & Berry, J. A. (1980). A biochemical model of photosynthetic CO₂ assimilation in leaves of C₃ species. *Planta*, 149(1), 78–90. <https://doi.org/10.1007/BF00386231>
- Felzer, B., Reilly, J., Melillo, J., Kicklighter, D., Sarofim, M., Wang, C., et al. (2005). Future effects of ozone on carbon sequestration and climate change policy using a global biogeochemical model. *Climatic Change*, 73(3), 345–373. <https://doi.org/10.1007/s10584-005-6776-4>
- Felzer, B. S., Cronin, T. W., Melillo, J. M., Kicklighter, D. W., & Schlosser, C. A. (2009). Importance of carbon-nitrogen interactions and ozone on ecosystem hydrology during the 21st century. *Journal of Geophysical Research*, 114(G1), G03009. <https://doi.org/10.1029/2009JG001083>

- Feng, Z., Pang, J., Kobayashi, K., Zhu, J., & Ort, D. R. (2011). Differential responses in two varieties of winter wheat to elevated ozone concentration under fully open-air field conditions. *Global Change Biology*, 17(1), 580–591. <https://doi.org/10.1111/j.1365-2486.2010.02184.x>
- Fensholt, R., Sandholt, I., & Rasmussen, M. S. (2004). Evaluation of MODIS LAI, fAPAR and the relation between fAPAR and NDVI in a semi-arid environment using in situ measurements. *Remote Sensing of Environment*, 91(3–4), 490–507. <https://doi.org/10.1016/j.rse.2004.04.009>
- Fiscus, E. L., Booker, F. L., & Burkey, K. O. (2005). Crop responses to ozone: Uptake, modes of action, carbon assimilation and partitioning. *Plant, Cell and Environment*, 28(8), 997–1011. <https://doi.org/10.1111/j.1365-3040.2005.01349.x>
- Francini, A., Nali, C., Picchi, V., & Lorenzini, G. (2007). Metabolic changes in white clover clones exposed to ozone. *Environmental and Experimental Botany*, 60(1), 11–19. <https://doi.org/10.1016/j.envexpbot.2006.06.004>
- Gong, C., Lei, Y., Ma, Y., Yue, X., & Liao, H. (2020). Ozone–vegetation feedback through dry deposition and isoprene emissions in a global chemistry–carbon–climate model. *Atmospheric Chemistry and Physics*, 20(6), 3841–3857. <https://doi.org/10.5194/acp-20-3841-2020>
- Grell, G., McKeen, S., Michalakes, J., Bao, J., Trainer, M., & Hsie, E. (2002). Real-time simultaneous prediction of air pollution and weather during the Houston 2000 Field Experiment. In *Paper presented at 4th conference on atmospheric chemistry: Atmospheric chemistry and Texas field study*.
- Grell, G. A., & Dévényi, D. (2002). A generalized approach to parameterizing convection combining ensemble and data assimilation techniques. *Geophysical Research Letters*, 29(14), 38-31–38-34. <https://doi.org/10.1029/2002GL015311>
- Guan, Q. (2019). *Observation and simulation of ozone dry deposition flux in summer maize field*, Master thesis, Nanjing University of Information Science & Technology (in Chinese). <https://doi.org/10.27248/d.cnki.gnjqc.2019.000142>
- Guenther, A., Karl, T., Harley, P., Wiedinmyer, C., Palmer, P. I., & Geron, C. (2006). Estimates of global terrestrial isoprene emissions using MEGAN (model of emissions of gases and Aerosols from nature). *Atmospheric Chemistry and Physics*, 6(11), 3181–3210. <https://doi.org/10.5194/acp-6-3181-2006>
- Herbinger, K., Then, C., Haberer, K., Alexou, M., Löw, M., Remele, K., et al. (2007). Gas exchange and antioxidative compounds in young beech trees under free-air ozone exposure and comparisons to adult trees. *Plant Biology*, 9(02), 288–297. <https://doi.org/10.1055/s-2006-924660>
- Hoshika, Y., Katata, G., Deushi, M., Watanabe, M., Koike, T., & Paoletti, E. (2015). Ozone-induced stomatal sluggishness changes carbon and water balance of temperate deciduous forests. *Scientific Reports*, 5(1), 9871. <https://doi.org/10.1038/srep09871>
- Huang, J., Zheng, Y., Xu, J., Zhao, H., Yuan, Y., & Chu, Z. (2016). O₃ dry deposition flux observation and soil resistance modeling over a bare soil in Nanjing. *Chinese Journal of Applied Ecology*, 10(10), 3196–3204. (in Chinese). <https://doi.org/10.13287/j.1001-9332.201610.001>
- Iacono, M. J., Delamere, J. S., Mlawer, E. J., Shephard, M. W., Clough, S. A., & Collins, W. D. (2008). Radiative forcing by long-lived greenhouse gases: Calculations with the AER radiative transfer models. *Journal of Geophysical Research*, 113(D13), D13103. <https://doi.org/10.1029/2008JD009944>
- Iriti, M., & Faoro, F. (2008). Oxidative stress, the paradigm of ozone toxicity in plants and animals. *Water, Air, and Soil Pollution*, 187(1–4), 285–301. <https://doi.org/10.1007/s11270-007-9517-7>
- Jin, Z., & Li, M. (2023). Effects of elevated ozone exposure on regional meteorology and air quality in China through ozone–vegetation coupling. [Dataset]. Zenodo. <https://doi.org/10.5281/zenodo.7762072>
- Kangasjärvi, J., Jaspers, P., & Kollist, H. (2005). Signalling and cell death in ozone-exposed plants. *Plant, Cell and Environment*, 28(8), 1021–1036. <https://doi.org/10.1111/j.1365-3040.2005.01325.x>
- Li, J., Mahalov, A., & Hyde, P. (2016). Simulating the impacts of chronic ozone exposure on plant conductance and photosynthesis, and on the regional hydroclimate using WRF/Chem. *Environmental Research Letters*, 11(11), 114017. <https://doi.org/10.1016/j.agrformet.2018.06.013>
- Li, K., Jacob, D. J., Shen, L., Lu, X., De Smedt, I., & Liao, H. (2020). Increases in surface ozone pollution in China from 2013 to 2019: Anthropogenic and meteorological influences. *Atmospheric Chemistry and Physics*, 20(19), 11423–11433. <https://doi.org/10.5194/acp-20-11423-2020>
- Li, L. Y., & Xie, S. D. (2014). Historical variations of biogenic volatile organic compound emission inventories in China, 1981–2003. *Atmospheric Environment*, 95, 185–196. <https://doi.org/10.1016/j.atmosenv.2014.06.033>
- Li, M., Liu, H., Geng, G., Hong, C., Liu, F., Song, Y., et al. (2017). Anthropogenic emission inventories in China: A review. [Dataset]. National Science Review, 4, 834–866. <https://doi.org/10.1093/nsr/nwx150>
- Li, M., Wang, T., Shu, L., Qu, Y., Xie, M., Liu, J., et al. (2021). Rising surface ozone in China from 2013 to 2017: A response to the recent atmospheric warming or pollutant controls? *Atmospheric Environment*, 246, 118130. <https://doi.org/10.1016/j.atmosenv.2020.118130>
- Li, M., Wang, T., Xie, M., Zhuang, B., Li, S., Han, Y., et al. (2017). Improved meteorology and ozone air quality simulations using MODIS land surface parameters in the Yangtze River Delta urban cluster, China. *Journal of Geophysical Research: Atmospheres*, 122(5), 3116–3140. <https://doi.org/10.1002/2016JD026182>
- Lombardozzi, D., Levis, S., Bonan, G., Hess, P., & Sparks, J. (2015). The influence of chronic ozone exposure on global carbon and water cycles. *Journal of Climate*, 28(1), 292–305. <https://doi.org/10.1175/JCLI-D-14-00223.1>
- Lombardozzi, D., Levis, S., Bonan, G., & Sparks, J. (2012). Predicting photosynthesis and transpiration responses to ozone: Decoupling modeled photosynthesis and stomatal conductance. *Biogeosciences*, 9(8), 3113–3130. <https://doi.org/10.5194/bg-9-3113-2012>
- Lombardozzi, D., Sparks, J., & Bonan, G. (2013). Integrating O₃ influences on terrestrial processes: Photosynthetic and stomatal response data available for regional and global modeling. *Biogeosciences*, 10(11), 6815–6831. <https://doi.org/10.5194/bg-10-6815-2013>
- Ma, N., Niu, G. Y., Xia, Y., Cai, X., Zhang, Y., Ma, Y., & Fang, Y. (2017). A systematic evaluation of Noah-MP in simulating land-atmosphere energy, water, and carbon exchanges over the continental United States. *Journal of Geophysical Research: Atmospheres*, 122(22), 12245–12268. <https://doi.org/10.1002/2017JD027597>
- McLaughlin, S. B., Nosal, M., Wullschleger, S. D., & Sun, G. (2007). Interactive effects of ozone and climate on tree growth and water use in a southern Appalachian forest in the USA. *New Phytologist*, 174(1), 109–124. <https://doi.org/10.1038/374252a0>
- Mills, G., Hayes, F., Wilkinson, S., & Davies, W. J. (2009). Chronic exposure to increasing background ozone impairs stomatal functioning in grassland species. *Global Change Biology*, 15(6), 1522–1533. <https://doi.org/10.1111/j.1365-2486.2008.01798.x>
- Misson, L., Panek, J. A., & Goldstein, A. H. (2004). A comparison of three approaches to modeling leaf gas exchange in annually drought-stressed ponderosa pine forests. *Tree Physiology*, 24(5), 529–541. <https://doi.org/10.1093/treephys/24.5.529>
- Morgan, P., Ainsworth, E., & Long, S. (2003). How does elevated ozone impact soybean? A meta-analysis of photosynthesis, growth and yield. *Plant, Cell and Environment*, 26(8), 1317–1328. <https://doi.org/10.1046/j.0016-8025.2003.01056.x>
- Myneni, R., Knyazikhin, Y., & Park, T. (2015). MCD15A2H MODIS/Terra+Aqua leaf area index/FPAR 8-day L4 global 500m SIN grid V006. [Dataset]. NASA EOSDIS Land Processes DAAC. <https://doi.org/10.5067/MODIS/MCD15A2H.006>
- Myneni, R. B., Hoffman, S., Knyazikhin, Y., Privette, J., Glassy, J., Tian, Y., et al. (2002). Global products of vegetation leaf area and fraction absorbed PAR from year one of MODIS data. *Remote Sensing of Environment*, 83(1–2), 214–231. [https://doi.org/10.1016/S0034-4252\(02\)00074-3](https://doi.org/10.1016/S0034-4252(02)00074-3)

- Niu, G. Y., Yang, Z. L., Mitchell, K. E., Chen, F., Ek, M. B., Barlage, M., et al. (2011). The community Noah land surface model with multiparameterization options (Noah-MP): 1. Model description and evaluation with local-scale measurements. *Journal of Geophysical Research*, 116(D12), D12109. <https://doi.org/10.1029/2010JD015139>
- NOAA. National Centers for Environmental Information. (2001). Global surface hourly. [Dataset]. NOAA National Centers for Environmental Information. Retrieved from <https://www.ncdc.noaa.gov/access/search/index>
- Noh, Y., Cheon, W., Hong, S., & Raasch, S. (2003). Improvement of the K-profile model for the planetary boundary layer based on large eddy simulation data. *Boundary-Layer Meteorology*, 107(2), 401–427. <https://doi.org/10.1023/A:1022146015946>
- Ollinger, S. V., Aber, J. D., Reich, P. B., & Freuder, R. J. (2002). Interactive effects of nitrogen deposition, tropospheric ozone, elevated CO₂ and land use history on the carbon dynamics of northern hardwood forests. *Global Change Biology*, 8(6), 545–562. <https://doi.org/10.1046/j.1365-2486.2002.00482.x>
- Pacifico, F., Folberth, G., Sitch, S., Haywood, J., Rizzo, L., Malavelle, F., & Artaxo, P. (2015). Biomass burning related ozone damage on vegetation over the Amazon forest: A model sensitivity study. *Atmospheric Chemistry and Physics*, 15(5), 2791–2804. <https://doi.org/10.5194/acp-15-2791-2015>
- Pan, X., Wang, Z., Wang, X., Dong, H., Xie, F., & Guo, Y. (2010). An observation study of ozone dry deposition over grassland in the suburban area of Beijing. *Chinese Journal of Atmospheric Sciences*, (01), 120–130.(in Chinese)
- Papanatsiou, M., Amtmann, A., & Blatt, M. R. (2017). Stomatal clustering in Begonia associates with the kinetics of leaf gaseous exchange and influences water use efficiency. *Journal of Experimental Botany*, 68(9), 2309–2315. <https://doi.org/10.1093/jxb/erx072>
- RDA. (2023). NCEP FNL operational model global tropospheric analyses, continuing from July 1999. [Dataset]. Research Data Archive at the National Center for Atmospheric Research, Computational and Information Systems Laboratory. <https://doi.org/10.5065/D6M043C6>
- Ren, W., Tian, H., Tao, B., Chappelka, A., Sun, G., Lu, C., et al. (2011). Impacts of tropospheric ozone and climate change on net primary productivity and net carbon exchange of China's forest ecosystems. *Global Ecology and Biogeography*, 20(3), 391–406. <https://doi.org/10.1111/j.1466-8238.2010.00606.x>
- Running, S., Mu, Q., & Zhao, M. (2015). MOD17A2H MODIS/Terra gross primary productivity 8-Day L4 global 500m SIN grid V006. [Dataset]. NASA EOSDIS Land Processes DAAC. <https://doi.org/10.5067/MODIS/MOD17A2H.006>
- Sadiq, M., Tai, A. P., Lombardozzi, D., & Val Martin, M. (2017). Effects of ozone–vegetation coupling on surface ozone air quality via biogeochemical and meteorological feedbacks. *Atmospheric Chemistry and Physics*, 17(4), 3055–3066. <https://doi.org/10.5194/acp-17-3055-2017>
- Sanderson, M., Jones, C., Collins, W., Johnson, C., & Derwent, R. (2003). Effect of climate change on isoprene emissions and surface ozone levels. *Geophysical Research Letters*, 30(18), 1936. <https://doi.org/10.1029/2003GL017642>
- Sitch, S., Cox, P., Collins, W., & Huntingford, C. (2007). Indirect radiative forcing of climate change through ozone effects on the land-carbon sink. *Nature*, 448(7155), 791–794. <https://doi.org/10.1038/nature06059>
- Skamarock, W. C., Klemp, J. B., Dudhia, J., Gill, D. O., Liu, Z., Berner, J., et al. (2019). A description of the advanced research WRF version 4.NCAR Tech. Note NCAR/TN-556-STR (p. 145). <https://doi.org/10.5065/dfn-6p97>
- Smith, A., Lott, N., & Vose, R. (2011). The integrated surface database: Recent developments and partnerships. *Bulletin of the American Meteorological Society*, 92(6), 704–708. <https://doi.org/10.1175/2011BAMS3015.1>
- Super, I., Vilà-Guerau de Arellano, J., & Krol, M. C. (2015). Cumulative ozone effect on canopy stomatal resistance and the impact on boundary layer dynamics and CO₂ assimilation at the diurnal scale: A case study for grassland in The Netherlands. *Journal of Geophysical Research: Biogeosciences*, 120(7), 1348–1365. <https://doi.org/10.1002/2015JG002996>
- Tai, A. P., Mickley, L. J., Heald, C. L., & Wu, S. (2013). Effect of CO₂ inhibition on biogenic isoprene emission: Implications for air quality under 2000 to 2050 changes in climate, vegetation, and land use. *Geophysical Research Letters*, 40(13), 3479–3483. <https://doi.org/10.1002/grl.50650>
- Thompson, G., Tewari, M., Ikeda, K., Tessendorf, S., Weeks, C., Otkin, J., & Kong, F. (2016). Explicitly-coupled cloud physics and radiation parameterizations and subsequent evaluation in WRF high-resolution convective forecasts. *Atmospheric Research*, 168, 92–104. <https://doi.org/10.1016/j.atmosres.2015.09.005>
- Tian, Y., Yao, X., Yang, J., Cao, W., Hannaway, D., & Zhu, Y. (2011). Assessing newly developed and published vegetation indices for estimating rice leaf nitrogen concentration with ground-and space-based hyperspectral reflectance. *Field Crops Research*, 120(2), 299–310. <https://doi.org/10.1016/j.fcr.2011.01.009>
- Val Martin, M., Heald, C., & Arnold, S. (2014). Coupling dry deposition to vegetation phenology in the Community Earth System Model: Implications for the simulation of surface O₃. *Geophysical Research Letters*, 41(8), 2988–2996. <https://doi.org/10.1002/2014GL059651>
- Val Martin, M., Heald, C., Lamarque, J.-F., Tilmes, S., Emmons, L., & Schichtel, B. (2015). How emissions, climate, and land use change will impact mid-century air quality over the United States: A focus on effects at national parks. *Atmospheric Chemistry and Physics*, 15(5), 2805–2823. <https://doi.org/10.5194/acp-15-2805-2015>
- Van Dingenen, R., Dentener, F. J., Raes, F., Krol, M. C., Emberson, L., & Cofala, J. (2009). The global impact of ozone on agricultural crop yields under current and future air quality legislation. *Atmospheric Environment*, 43(3), 604–618. <https://doi.org/10.1016/j.atmosenv.2008.10.033>
- Verstraeten, W. W., Neu, J. L., Williams, J. E., Bowman, K. W., Worden, J. R., & Boersma, K. F. (2015). Rapid increases in tropospheric ozone production and export from China. *Nature Geoscience*, 8(9), 690–695. <https://doi.org/10.1038/ngeo2493>
- Warrach-Sagi, K., Ilgwersen, J., Schwitalla, T., Troost, C., Aurbacher, J., Jach, L., et al. (2022). Noah-MP with the generic crop growth model Gcros in the WRF model: Effects of dynamic crop growth on land-atmosphere interaction. *Journal of Geophysical Research-Atmospheres*, 127(14). <https://doi.org/10.1029/2022JD036518>
- Wei, L. (2019). *Comparison of observations on the characteristics of ozone deposition in winter wheat and maize*, Master thesis, Nanjing University of Information Science & Technology (in Chinese). <https://doi.org/10.27248/d.cnki.gnjqc.2019.000089>
- Wesely, M. (2007). Parameterization of surface resistances to gaseous dry deposition in regional-scale numerical models. *Atmospheric Environment*, 41(6), 52–63. [https://doi.org/10.1016/0004-6981\(89\)90153-4](https://doi.org/10.1016/0004-6981(89)90153-4)
- Wild, O., Fiore, A. M., Shindell, D., Doherty, R., Collins, W., Dentener, F., et al. (2012). Modelling future changes in surface ozone: A parameterized approach. *Atmospheric Chemistry and Physics*, 12(4), 2037–2054. <https://doi.org/10.5194/acp-12-2037-2012>
- Wittig, V. E., Ainsworth, E. A., & Long, S. P. (2007). To what extent do current and projected increases in surface ozone affect photosynthesis and stomatal conductance of trees? A meta-analytic review of the last 3 decades of experiments. *Plant, Cell and Environment*, 30(9), 1150–1162. <https://doi.org/10.1111/j.1365-3040.2007.01717.x>
- Wu, K., Yang, X., Chen, D., Gu, S., Lu, Y., Jiang, Q., et al. (2020). Estimation of biogenic VOC emissions and their corresponding impact on ozone and secondary organic aerosol formation in China. *Atmospheric Research*, 231, 104656. <https://doi.org/10.1016/j.atmosres.2019.104656>

- Wu, L., Long, T.-y., Liu, X., & Guo, J.-s. (2012). Impacts of climate and land-use changes on the migration of non-point source nitrogen and phosphorus during rainfall-runoff in the Jialing River Watershed, China. *Journal of Hydrology*, 475, 26–41. <https://doi.org/10.1016/j.jhydrol.2012.08.022>
- Xiao, M., Zhu, J., Feng, L., Liu, C., & Xing, W. (2015). Meso/macroporous nitrogen-doped carbon architectures with iron carbide encapsulated in graphitic layers as an efficient and robust catalyst for the oxygen reduction reaction in both acidic and alkaline solutions. *Advanced Materials*, 27(15), 2521–2527. <https://doi.org/10.1002/adma.201500262>
- Xie, X., Wang, T., Yue, X., Li, S., Zhuang, B., Wang, M., & Yang, X. (2019). Numerical modeling of ozone damage to plants and its effects on atmospheric CO₂ in China. *Atmospheric Environment*, 217, 116970. <https://doi.org/10.1016/j.atmosenv.2019.116970>
- Xu, J., Zheng, Y., Mai, B., Zhao, H., Chu, Z., Huang, J., & Yuan, Y. (2018). Simulating and partitioning ozone flux in winter wheat field: The Surfamt-O3 model. *China Environmental Science*, (02), 455–470. (in Chinese). <https://doi.org/10.19674/j.cnki.issn1000-6923.2018.0053>
- Yang, T., Liu, H., Wang, X., Peng, Z., & Yu, B. (2021). Impacts of urban vegetation on air pollutant concentration in Hangzhou. *The Administration and Technique of Environmental Monitoring*, 33(3), 15–20. <https://doi.org/10.19501/j.cnki.1006-2009.2021.03.004>
- Yoon, J. W., Lim, S., & Park, S. K. (2021). Combinational optimization of the WRF physical parameterization schemes to improve numerical sea breeze prediction using micro-genetic algorithm. *Applied Sciences-Basel*, 11(23), 11221. <https://doi.org/10.3390/app112311221>
- Yue, X., Unger, N., Harper, K., Xia, X., Liao, H., Zhu, T., et al. (2017). Ozone and haze pollution weakens net primary productivity in China. *Atmospheric Chemistry and Physics*, 17(9), 6073–6089. <https://doi.org/10.5194/acp-17-6073-2017>
- Zaveri, R. A., Easter, R. C., Fast, J. D., & Peters, L. K. (2008). Model for simulating aerosol interactions and chemistry (MOSAIC). *Journal of Geophysical Research*, 113(D13), D13204. <https://doi.org/10.1029/2007JD008782>
- Zaveri, R. A., & Peters, L. K. (1999). A new lumped structure photochemical mechanism for large-scale applications. *Journal of Geophysical Research*, 104(D23), 30387–30415. <https://doi.org/10.1029/1999JD900876>
- Zheng, B., Tong, D., Li, M., Liu, F., Hong, C., Geng, G., et al. (2018). Trends in China's anthropogenic emissions since 2010 as the consequence of clean air actions. [Dataset]. *Atmospheric Chemistry and Physics*, 18, 14095–14111. <https://doi.org/10.5194/acp-18-14095-2018>
- Zhu, J., Tai, A. P., & Hung Lam Yim, S. (2022). Effects of ozone–vegetation interactions on meteorology and air quality in China using a two-way coupled land–atmosphere model. *Atmospheric Chemistry and Physics*, 22(2), 765–782. <https://doi.org/10.5194/acp-22-765-2022>
- Zhu, Z., Sun, X., Zhao, F., & Meixner, F. X. (2015). Ozone concentrations, flux and potential effect on yield during wheat growth in the Northwest-Shandong Plain of China. *Journal of Environmental Sciences*, 34, 1–9. <https://doi.org/10.1016/j.jes.2014.12.022>